LOW FRICTION TRIBOFILM FORMATION AND DISTRIBUTION ON AN ENGINE CYLINDER TESTED WITH MoDTC-CONTAINING LOW VISCOSITY ENGINE LUBRICANTS

Gerda Vaitkunaite [a], Cayetano Espejo [a], Benoît Thiebaut [b], Anne Neville [a], Ardian Morina [a]

a School of Mechanical Engineering, University of Leeds, Leeds, LS2 9JT, UK

b TOTAL, Solaize Researcher Center, Cedex, BP22-69360, France

KEY STATEMENTS:

- MoS_2 tribofilm spatial distribution influences the friction force in the piston-liner tribological contact.
- MoS_2 tribofilm coverage in the liner is highest at the ring reversal point at the BDC, where boundary lubrication is expected.
- MoS_2 formation was also detected at a narrow location in the middle part of the stroke. Therefore, MoS_2 formation in the middle of the liner could be attributed to the piston secondary motion effect.
- MoDTC effect was not observed at the TDC area, regardless of the MoDTC concentration in the lubricant.

ABSTRACT

The piston-liner tribological contact has a key role in controlling friction caused energy losses in a passenger car engine. This study analyses the MoDTC-containing low viscosity lubricant performance and the resulting low-friction MoS_2 tribofilm distribution on the liner surface. The engine liners were tested in a floating liner measurement system, where fully-formulated lubricants with different MoDTC concentrations were utilised to assess the impact of friction modifiers on the friction performance. Tested engine liners were dismantled from the measurement system, and MoS_2 tribofilm formation on the liner was quantitatively characterised by Raman Microscopy mapping. The MoS_2 tribofilm chemical composition and lamellar structure were further investigated by Transmission Electron Microscopy (TEM), High-Angle Annular Dark-Field Scanning (HAADF) and Energy Dispersive X-ray (STEM-EDX) Microscopy. The findings presented in this paper confirm that MoS_2 tribofilm spatial distribution plays a pivotal role in reducing friction in piston-liner contact. 60% friction torque reduction was achieved at BDC area with 0.7% MoDTC concentration in the fully formulated lubricant. Moreover, MoS_2 presence in the middle of the liner indicates MoDTC effectiveness throughout the whole engine cycle. Therefore, contributing to the overall energy savings in passenger cars.

1. INTRODUCTION

Transport activities account for 30% of greenhouse gas emissions [1], [2]. However, in passenger vehicles, only 21% of the fuel is used for car movement. The remaining 79% of energy is wasted through overcoming friction, exhaust and cooling losses in the internal combustion engine [3]–[5]. Therefore, it is essential to optimise the energy savings in internal combustion engines by improving lubrication in tribological engine contacts.

The improvements in engine lubricants and following prevention of energy loss can be accomplished by lowering lubricant viscosity. However, the oil viscosity reduction in the engine causes oil pumps, bearings, and piston assembly to operate in boundary and mixed lubrication regimes [4]–[6]. Additionally, a lower engine oil viscosity in the cylinder block leads to higher friction and wear in the top dead and bottom dead centre areas at the reversal points of the piston ring [7]. Thus, the tribological conditions along the piston stroke strongly influence the overall engine performance. Furthermore, the piston movement in the cylinder liner is reported to cause 50% of all friction losses in the piston-liner system [8].

The future engine oils are challenged to deliver high performance in both engine starting and stopping stages by protecting component surfaces from wear and reducing the friction in the rubbing contacts. Unfortunately, these conditions exacerbate the problems associated with the engine running simultaneously in different lubrication regimes. As a result, engine components are subjected to overheating and excessive wear due to extreme engine running conditions.

Friction and anti-wear additives in engine oils effectively protect the surface of the engine components and reduce friction. For example, the Molybdenum Dithiocarbamate (MoDTC) friction modifier decomposes under severe tribological conditions, therefore providing friction reduction. The friction reduction mechanism is based on MoDTC molecule chemical bonds rupture and 2D MoS_2 nanosheets formation during boundary lubrication conditions. The reduction of friction is obtained in tribometer testing conditions [9]–[11] and engine tests [12], due to low friction MoS_2 sheets formation in the tribological contact area.

Raman microscopy is one of the most suitable techniques to determine the presence of $MoS_2,$ considering a typical tribofilm thickness of 100 nm [11], [13]. MoS_2 distinct peaks appear in Raman spectra at 383 cm^{-1} and 408 cm^{-1} Raman shift, corresponding to A_{1g} and E^1_{2g} vibrational modes [9]–[11]. Raman Microscopy based characterisation of engine components, conducted by Espejo et al. [12], showed that even a small amount of MoDTC in the fully formulated lubricant could lead to MoS_2 formation in the engine and significantly impact the friction performance. In their work, MoS_2 formation was detected at the Bottom Dead Centre (BDC) area and near the Top Dead Centre (TDC) area on the liner. In addition, some MoS_2 species are found at the oil ring reversal point, whereas the middle of the stroke did not exhibit MoS_2 formation. Therefore, MoS_2 formation was detected only at the reversal points of the piston rings where boundary lubrication is expected. However, there is little knowledge of MoS_2 tribofilm distribution and thickness formed on the engine liner and its effect on the overall engine friction performance.

Therefore, the current paper aims to characterise and quantify the MoS_2 tribofilms formed in the piston-cylinder tribological contact during floating liner tests to assess the frictional performance of low viscosity fully formulated oils with different MoDTC concentrations.

2. EXPERIMENTAL METHODOLOGY

2.1 Floating liner engine tests

Experimental tests were conducted using a low viscosity fully-formulated (FF) oil from a group III base stock with High Temperature High Shear (HTHS) viscosity of 2.1 cP. Oils were blended with 0.1 wt%, 0.3 wt%, 0.5 wt% and 0.7 wt% MoDTC friction modifier, equivalent to 100 ppm, 300 ppm, 500 ppm and 700 ppm of molybdenum in the oil. The chemical composition of the lubricants used in the study are given in Table 1.

Table 1. Fully formulated lubricant chemistry and resulting viscosity parameters.

	FF Oil 2
Additive package (wt, %)	12.3
Viscosity modifier (wt, %)	4
Base oil, group III (wt, %)	82
Kinematic viscosity of the base oil at 100°C (cSt)	3
HTHS at 150°C (cP)	2.1
Pressure-Viscosity Coefficient, GPa^{-1}	9.7
Dynamic viscosity at 90°C (η_o, Pa s)	$5.76 \cdot 10^{-3}$
Dynamic viscosity at 100°C (η_o, Pa s)	$4.76 \cdot 10^{-3}$
MoDTC concentration (wt%)	0.1-0.7

These oils were tested in AVL FRISC Floating Liner Engine. The detailed floating liner measurement system description has been previously presented by AVL List GmbH in [14]–[16]. The floating liner testing method enables single-cylinder engine testing in fired conditions with a gasoline direct injection (GDI) combustion system adapted from passenger cars.

The simplified scheme of the floating liner system is shown in **Figure 1** a). First, the single-cylinder is sealed and placed in the customised crankcase to fit friction measurement sensors. Then, the liner is fitted with three-component piezoelectric load cells force sensors to directly measure the friction force between piston and cylinder liner interfaces. The detailed piston-cylinder liner interface cross-section and main design elements such as cylinder head, sensor package and piston rings are shown in **Figure 1** b).
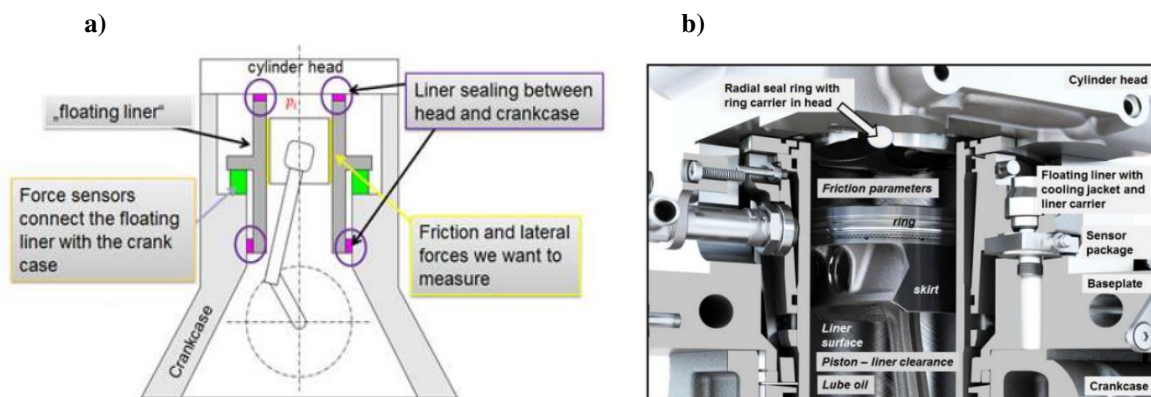

Figure 1 a) Simplified scheme of the floating liner measurement system, b) piston-cylinder liner interface cross-section and detailed component layout of the "FRISC" floating liner single-cylinder engine [15], [16].

Before testing each oil, the hardware and new liners are installed in the crankcase. Next, the whole system is cleaned to remove residual oil from the floating liner and avoid contamination. To clean each cylinder liner a standard detergent was used, without any additional lubricant additives. Before testing each oil, one flush run were carried out to remove all possible contamination from manufacturing and assembly processes. Afterwards, the oil filters are changed after each engine flush runs to avoid system contamination. The simplified testing procedure sequence is given in Figure 2, and testing conditions are given in Table 2. The friction force measurements are recorded for 1 hour. The friction force averaging value during one engine cycle that consists of intake, compression, combustion and exhaust strokes is then plotted against the crankshaft angle.

The tests were conducted with a grey cast iron cylinder liner at 1200 rpm engine speed, 6.5 bar pressure, and an oil temperature of 90 °C. The first piston ring was coated with chrome-nitride coating and the second piston ring was coated with PVD-phosphate. The same piston rings were kept for all engine tests presented in this paper. The experimental parameters and testing sequence for the floating liner measurements are summarised in Tables 2 and 3, respectively. Firstly, the reference test was made to assess friction behaviour in the engine with low viscosity oil. Next, liners 1 - 4 were tested in the same low viscosity oil, except adding additional different MoDTC concentrations of 0.1, 0.3, 0.5 and 0.7wt%, respectively. The liner designation and MoDTC concentration of each floating liner measurements are given in Table 3.
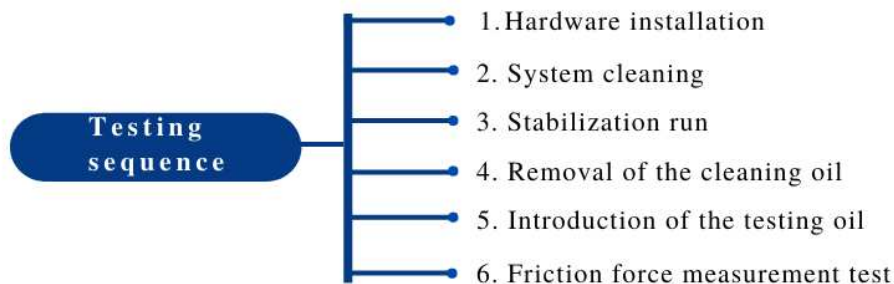
Figure 2 Oil testing procedure in the floating liner engine.

Table 2 Fired engine test parameters in the floating liner measurement system.

Oil temperature	90 °C
Temperature at the liner surface	130°C (TDC) - 107°C (BDC)
Engine speed	1200 rpm
Pressure on the cylinder head	6.5 bar

Table 3 Testing sequence in the floating liner measurement system.

Liner sequence	MoDTC concentration in the lubricant (wt %)
Liner reference	FFO
Liner 1	FFO + 0.7 MoDTC, %

Liner 2	FFO + 0.5 MoDTC, %
Liner 3	FFO + 0.3 MoDTC, %
Liner 4	FFO + 0.1 MoDTC, %

2.2 Sample preparation and visual inspection

After the tests, the liners were removed from the floating liner system, and the surface was inspected. Figure 3 shows the liner removed after a floating liner engine test. The image of the liner is presented in Figure 3 a). First, liners were cut into two halves, as shown in Figure 3 b). During the cutting process, the liner surface was blasted with compressed air making sure that the analysis area was not affected by surface contamination by debris and avoiding the thermal effect of the cutting. Therefore, the cutting process was carried out under dry conditions, and no lubricants were used during the cutting process to avoid possible contamination of the surface.

Next, the liner was then cut into thin samples along the stroke to provide better access for wear and surface chemistry characterisation and comply with microscope sample size requirements. The extracted sample width was 15 mm, and the sample length was 120 mm. The detailed dimensions of the extracted samples are given in Figure 4.

Scanning Electron Microscope (Carl Zeiss EVO MA15) equipped with Energy Dispersive X-Ray (EDX) spectrometer (Oxford Instruments) was used to evaluate cylinder liner surface wear. Combined with EDX mapping, provided chemical information on the tribofilm formation on the observed wear regions.
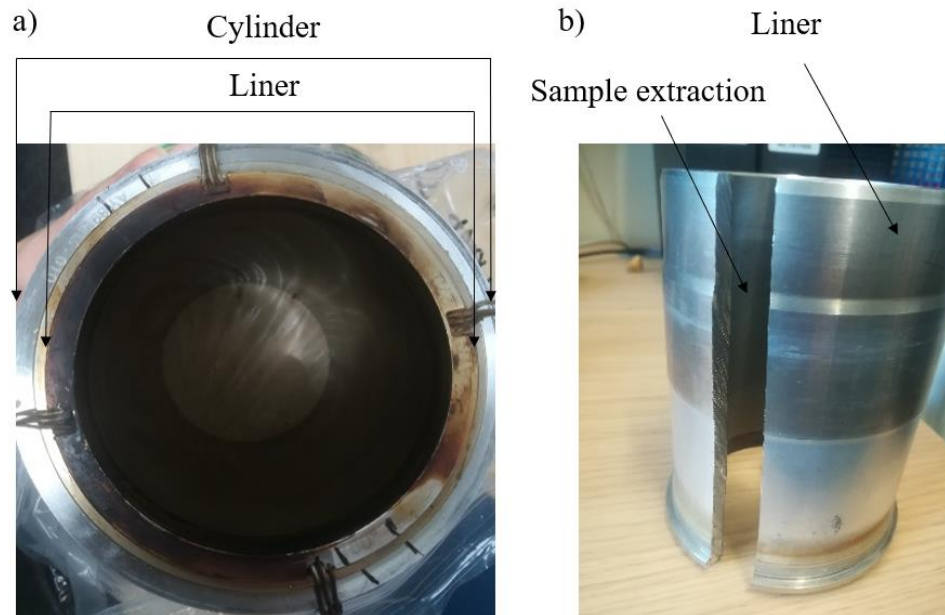

Figure 3 a) Cylinder removal after the test in floating liner measurement system. b) liner removal from the cylinder and sample extraction.

2.3 MoS$_2$ tribofilm surface chemistry characterisation

Raman analysis was conducted by obtaining Raman maps from the TDC to the BDC at 1 cm intervals along the piston stroke (Figure 4 a)). Two samples were extracted to assess wear and MoS_2 tribofilm distribution differences along the circumference of the liner: one from the thrust side and another from the anti-thrust side, as displayed in Figure 4 b). Figure 4 c) shows the extracted engine samples, and residual oil cutting debris was removed with heptane.

Raman microscopy (inVia Renishaw system) was used to identify the tribofilm formation on the liner surface and characterise spatial distribution of the MoS_2 formed during the fired engine test. The laser excitation source was a 488 nm wavelength laser combined with a 2400 lines/mm grating mirror and a CCD detector to deliver a spectral resolution of 1 cm^{-1}. The laser and spectrometer was combined with a Leica confocal optical microscope mounting 50x objective lens, which provides a 1 μm lateral resolution. Raman laser power of 3.3 mW was selected to avoid damage and thermal energy influence on the tribofilm formed on the liner.

The tribofilm quality and spatial distribution are then correlated to the friction performance.
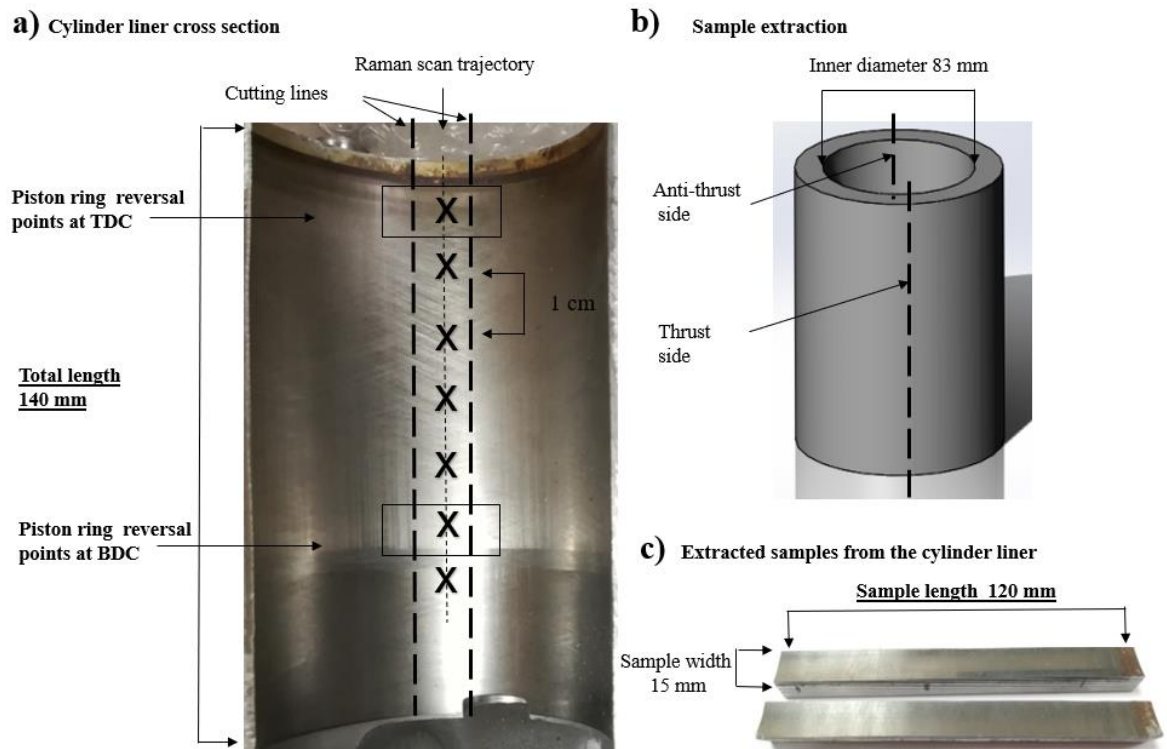

Figure 4 Liner sample preparation a) cylinder liner cross-section showing chemical analysis pathway from TDC to BDC, b) sample extraction from the engine anti-thrust and thrust sides and sample next to the thrust side, c) extracted engine samples to comply with the microscope chamber sample requirements.

2.4 MoS$_2$ tribofilm quantitative analysis on engine components

MoS$_2$ spatial distribution was evaluated by Raman mapping. The Raman map is an analysis delivering a 2D contour plot presentation of the intensity counts of the tribofilm based on the most dominant A_{1g} peak spectral region. The automated stage in the Raman system allows the collection of chemical surface information from the predefined areas on the liner surface. Raman mapping was set to scan a 50 μm x 30 μm area

along the x-axis and y-axis directions, shifting the scanning area in equal distances between BDC and TDC. Figure 5**Figure** a) shows the optical microscope image from the liner surface with typical honing lines at the BDC area and an example of the mapping mesh grid. The circular regions at the intersection point, shown in Figure 5 b), are laser source spots from which Raman spectra were acquired. The typical Raman spectra of MoS_2 is shown in Figure 5 c). Figure 5 d) shows the corresponding Raman map developed, where each colour pixel in the Raman map represents the A_{1g} intensity counts acquired from the Raman spectra. The pixel's colour was determined from a colour scale where low-intensity values were blue, and high-intensity values were yellow. The white colour in the map shows areas where no MoS_2 peaks were observed, equivalent to 0 intensity counts in the A_{1g} peak spectral region.

Metal surfaces after tribological tests are known to produce fluorescence in the Raman spectra, which hinders peak acquisition, as Raman peaks can be entirely overshadowed by fluorescence background. Furthermore, fluorescence in the Raman spectra is especially prominent on engine component surfaces [12], [17]. Therefore, the background effects were removed from Raman spectra by an open-source statistical computing program R. Next, the MoS_2 peaks in Raman spectra were fitted according to the Gaussian filter. Finally, MoS_2 presence was considered in the pixel when A_{1g} peak intensity in the Raman spectra exceeded 10 counts.

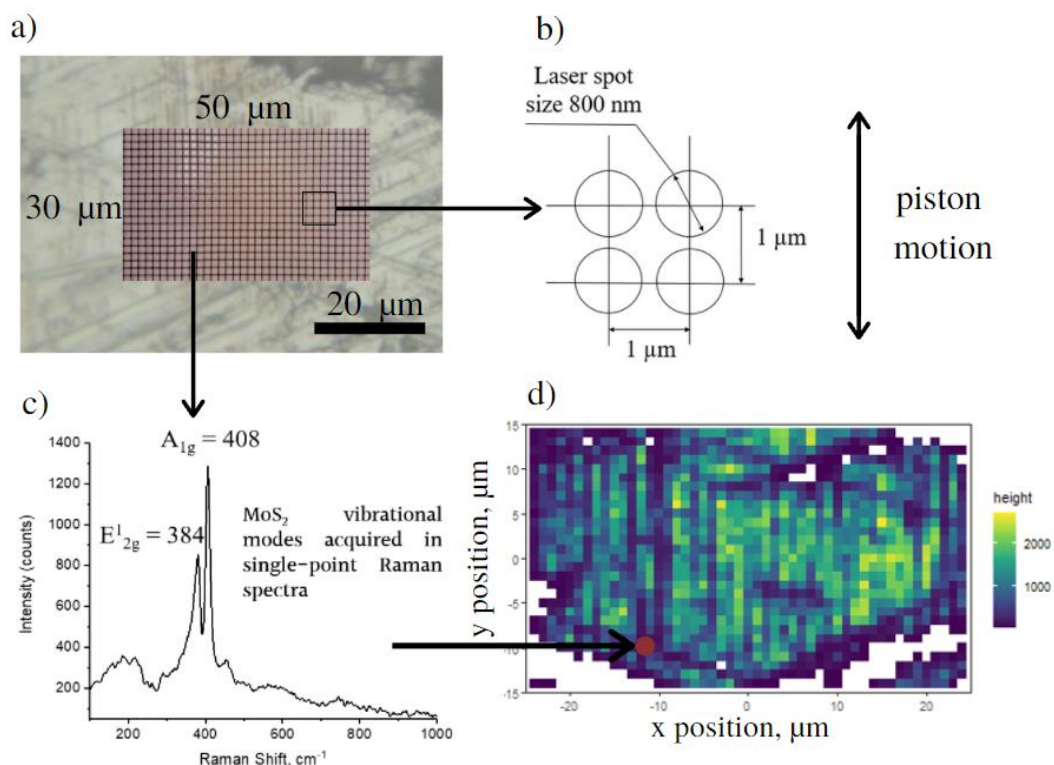**Figure 5 Development of Raman mapping on the liner surface a) an optical image of the analysed area on the liner BDC area and schematic diagram showing a mesh created over an area measuring 50 μm x 30 μm, b) single unit dimensions used to create 1 μm x 1 μm of the Raman map, c) single-spot Raman spectra representing MoS_2 vibrational modes, d) MoS_2 tribofilm Raman map based on A_{1g} peak spectral region.**

After Raman mapping, the MoS$_2$ tribofilm intensity 2D area coverage and cumulative intensity histogram were calculated. Figure 6 shows how the histogram is built. The histograms represent the frequency of Raman map points with an intensity falling within a particular interval or bin. For this study, a class interval of 100 counts was selected to build the histograms. For example, in Figure 6 c), the first bin indicates 350 out of the 1581 acquired points with Raman A$_{1g}$ peak intensities of 0 to 99 counts (Figure 6 b). The second bin indicates 160 points with Raman intensities of 100 to 199 counts.

To quantify MoS$_2$ species detected in each Raman map and histogram, area coverage, cumulative intensity, intensity average (mean) and standard deviation parameters were calculated according to the intensity counts acquired during the map scan. Equation (1) defines calculations for MoS$_2$ 2D area coverage. First, pixels representing MoS$_2$ presence were divided by the total number of pixels in the map. Then, the cumulative intensity was calculated from all intervals and frequencies in Equation (2). The cumulative intensity ($\sum$) was obtained from all Raman peak intensities detected during the map scan. Finally, the frequency per mapping intensity was plotted and correlated depending on the piston motion on the liner.
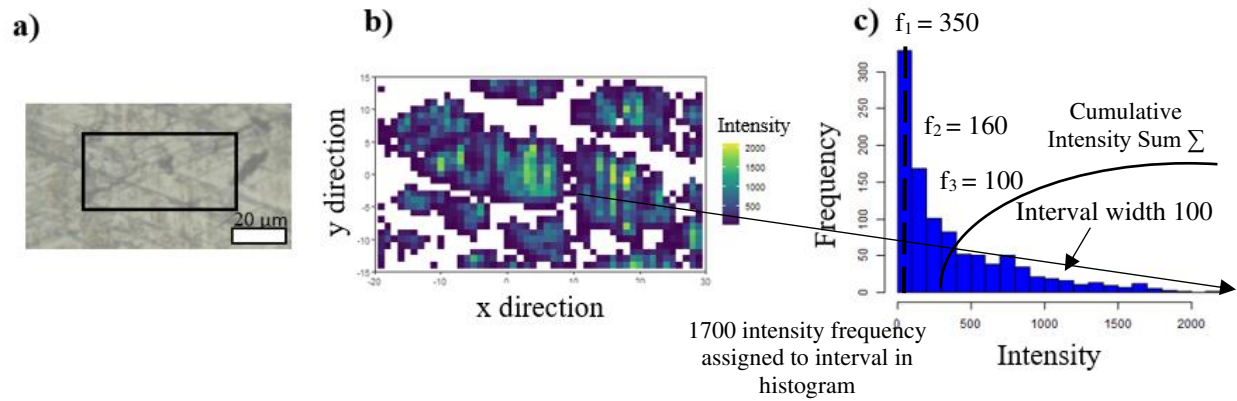

Figure 6 a) optical image of the liner surface, b) Raman map of the MoS$_2$ tribofilm based on A$_{1g}$ peak b) Raman map conversion to histogram according to A$_{1g}$ peak intensity.

$$2D\ Area\ Coverage\ (\%) = \frac{Number\ of\ pixels\ with\ MoS_2\ peaks}{Total\ number\ of\ pixels\ in\ map} x100;\ (1)$$

$$\sum = 200 \cdot f_1 + 400 \cdot f_2 + 600 \cdot f_3 + \cdots n \cdot f_n\ ;\ (2)$$

2.5 MoS$_2$ tribofilm structural analysis

Figure 7 shows the procedure developed for MoS$_2$ tribofilm identification on the surface of engine components analysed. Firstly, Raman mapping identified the MoS$_2$ tribofilm location on the surface (Figure 7 a). Next, the formation region was micro-indented for reference of the analysis area, and a cross-section sample was extracted from the engine sample. Next, the tribofilm cross-sections were prepared with Focused Ion Beam (FIB, Helios G4 CX Dual Beam) milling. Finally, prepared tribofilm cross-sections were analysed with

Scanning Transmission Electron Microscopy (STEM), High-Angle Annular Dark-Field Scanning (HAADF) and Energy Dispersive X-ray (EDX) methods.

Figure 7 b) shows electron beam transmission through MoS_2 tribofilm cross-section sample and construction of HAADF imaging used for EDX analysis. The tribofilm cross-sections milling was chosen to avoid high-intensity substrate peak acquisition in the EDX spectra.
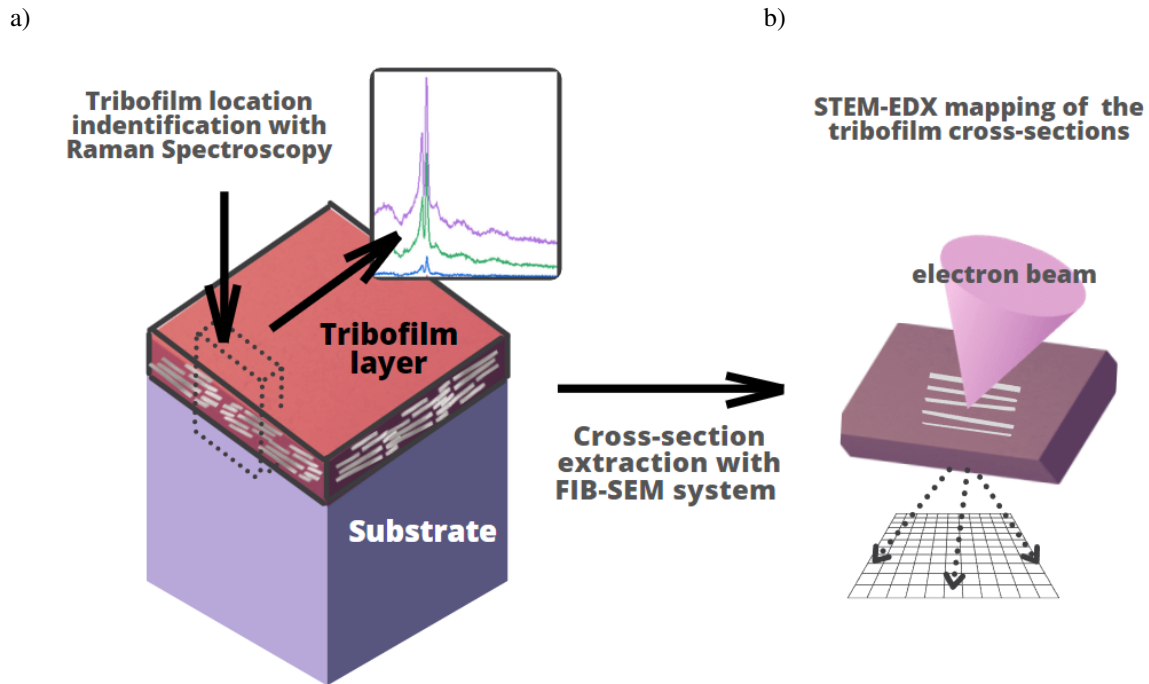
a)   b)

Figure 7 HAADF STEM-EDX method application to MoS₂ tribofilm characterisation.

3 RESULTS

3.1 Analysis of the friction behaviour at piston-liner contact

Friction results are obtained from the previously described floating liner measurement method. Figure 8 shows friction force measurements recorded at the piston-liner contact during 1 hour tests. Tests were carried out with different MoDTC concentrations in the lubricant and constant engine operating conditions as previously presented in Tables 1 and 2. The friction force curve represents the average friction force value during one engine cycle. The depicted engine cycle starts at the TDC area with the intake stroke when the piston moves down to the BDC area. Then, the piston travels back towards TDC, compressing the air-fuel mixture, followed by combustion (TDC to BDC) and exhaust (BDC to TDC) strokes.

Figure 8 shows that the highest friction reduction was achieved at the BDC region when testing 0.5wt% MoDTC and 0.7wt% MoDTC lubricants. Generally, all tested lubricants containing MoDTC exhibited lower friction force at the BDC region than the reference test without MoDTC. Higher MoDTC concentration leads to

higher friction reduction. However, the differences in friction force reduction between 0.3%-0.7% MoDTC concentrations are minor. Additionally, even a small concentration of 0.1 wt% MoDTC in the lubricant leads to a friction reduction; however, observed values are very close to values obtained from the FF lubricant test.

MoDTC influence on friction is most substantial at the BDC area, where the boundary lubrication regime occurs. However, regardless of the MoDTC quantity in the oil, no significant friction reduction was reported at the TDC area, attributed to thermal oil degradation [12]. It is worth mentioning that the MoDTC effect is evident in the middle of the stroke, despite the higher piston speed, resulting in a less severe boundary lubrication regime, shifting towards a mixed and hydrodynamic lubrication regime [18].
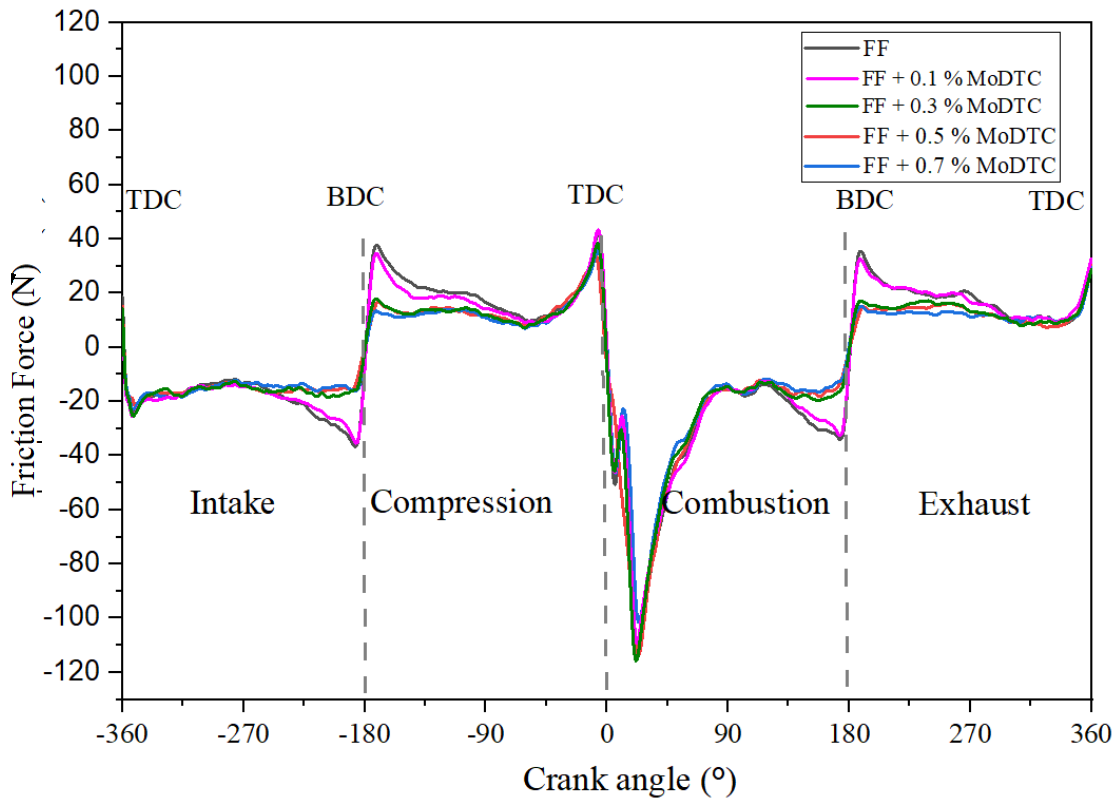

Figure 8 Comparison of the different MoDTC concentration influence on the averaged friction force measurements during 1 hour tests in the floating liner.

Different friction behaviour was observed in the BDC, middle, and TDC positions in the piston-cylinder contact. Therefore, Raman Microscopy characterisation was employed to evaluate MoS_2 tribofilm distribution on different locations on the liner.

3.2 Liner wear after floating liner engine test

SEM images in Figure 9 **Error! Reference source not found.**shows textured liner surface after the fired floating liner tests. Figure 9 a) indicates that the TDC region is slightly more polished after floating liner tests

than well-maintained honing grooves in the middle of the liner (Figure 9 b)). Honing grooves are partially removed and worn out in the BDC area, slightly above the piston ring reversal point (Figure 9 c)), revealing an overall smoother surface.

Abrasive wear generated by piston ring sliding is observed in TDC and BDC areas in the form of axial scratches, shown in Figures 9 a) and c). No distinct wear was observed in the middle of the liner, where less severe lubrication conditions are experienced (Figure 9 b)). Abrasive wear is typical for liner when entering boundary lubrication conditions [19]–[22]. The axial scratches in the BDC area are considerably less apparent than those in the TDC area, which were previously reported by Filho et al. [22] and in agreement with cylinder topography studies conducted by Dimkovski et al. [23].

Material removal and voids are observed in all three analysed areas indicating material loss due to piston sliding. In addition, visible micro pits are distributed uniformly along the whole liner surface, indicating possible micro pits formation during manufacturing and machining of the liner. The micro pits caused by the manufacturing process were not removed by the honing process or piston sliding since the micro pits are distributed uniformly rather than along the piston motion direction. Similar manufacturing caused pits were previously observed by Papadopoulos et al. [19].
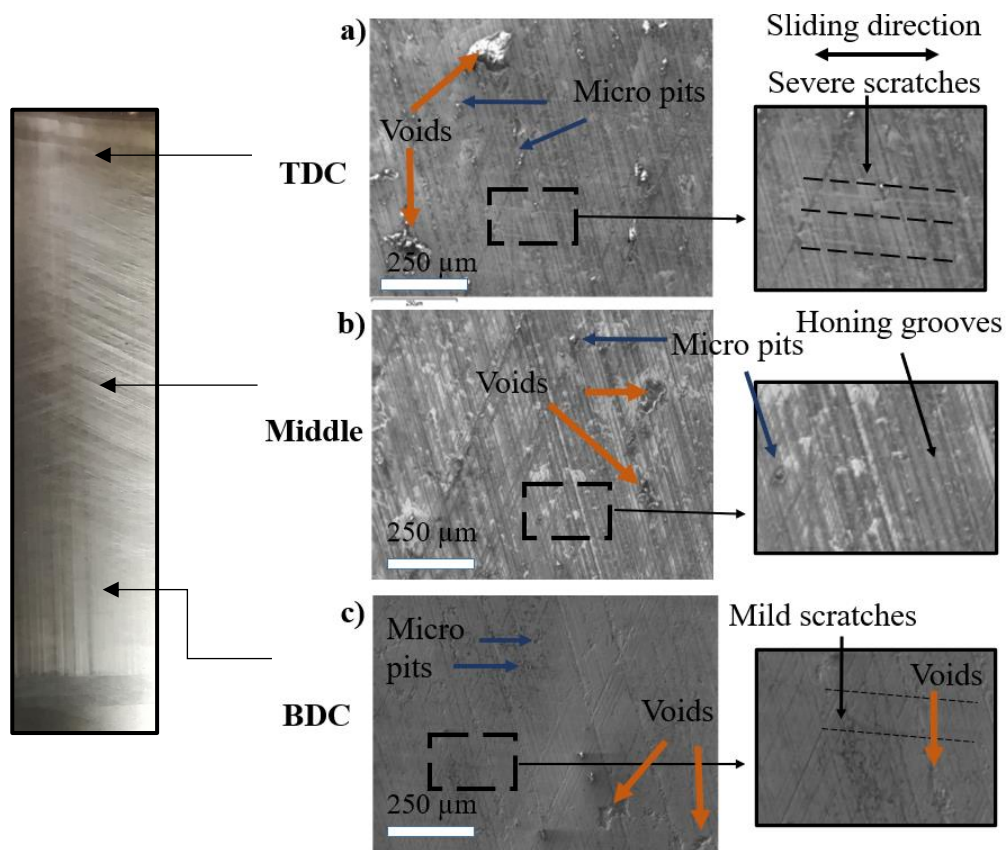

Figure 9 SEM images of the worn surfaces at a) TDC area, below the highest point of the piston ring reverse, b) middle of the liner, c) BDC area, above the reversal point of the ring sliding.

3.3 MoS₂ tribofilm chemical composition

Figure 10 shows single Raman spectra acquired from the Liner 2 (tested with 0.5% MoDTC) BDC area, the middle of the liner and TDC area. All Raman spectra are shifted vertically for presentation purposes, revealing MoS$_2$ peaks in all three positions on the cylinder. Raman signal-to-noise ratio was low in the middle of the liner and TDC areas due to the lower MoS$_2$ content.

The spectrum from the BDC area shown in Figure 10 has sharp MoS$_2$ peaks at 409 cm^{-1} and 380 cm^{-1} corresponding to E$^1_{2g}$ and A$_{1g}$ bands, respectively [9], [24]. The broad, amorphous peak at 100-250 cm^{-1} is assigned to stress-induced distortion in MoS$_2$ structure [10], 293 cm^{-1} is ascribed to MoS$_2$ first order E$_{1g}$ peak [25], the shoulder peak at 330 cm^{-1} and peak 459 cm^{-1} is identified as MoS$_x$ formation [9]. MoS$_x$ peaks are low intensity in comparison to MoS$_2$ peaks in the BDC area. On the opposite side, MoS$_x$ peaks appear in higher intensity in the middle of the liner and TDC area scans. Increased MoS$_x$ intensity in the middle of the liner can be caused by lower contact pressure in the middle of the liner as MoS$_x$ forms under lower shear stresses than MoS$_2$ [9]. Moreover, this is the first time MoS$_2$ formation has been observed in the middle of the liner when piston speed is the highest.

Previously, Espejo et al. [12] reported MoS$_2$ tribofilm formation in a motored engine test. In their work, distinct MoS$_2$ peaks were observed in the BDC area. Moreover, in the TDC area, a low-intensity MoS$_2$ signal was obtained. Therefore, recorded low-intensity signal acquisition and a high spectral fluorescence obtained from the TDC area and middle of the cylinder were assigned to engine oil thermal degradation and resulting carbon formation.
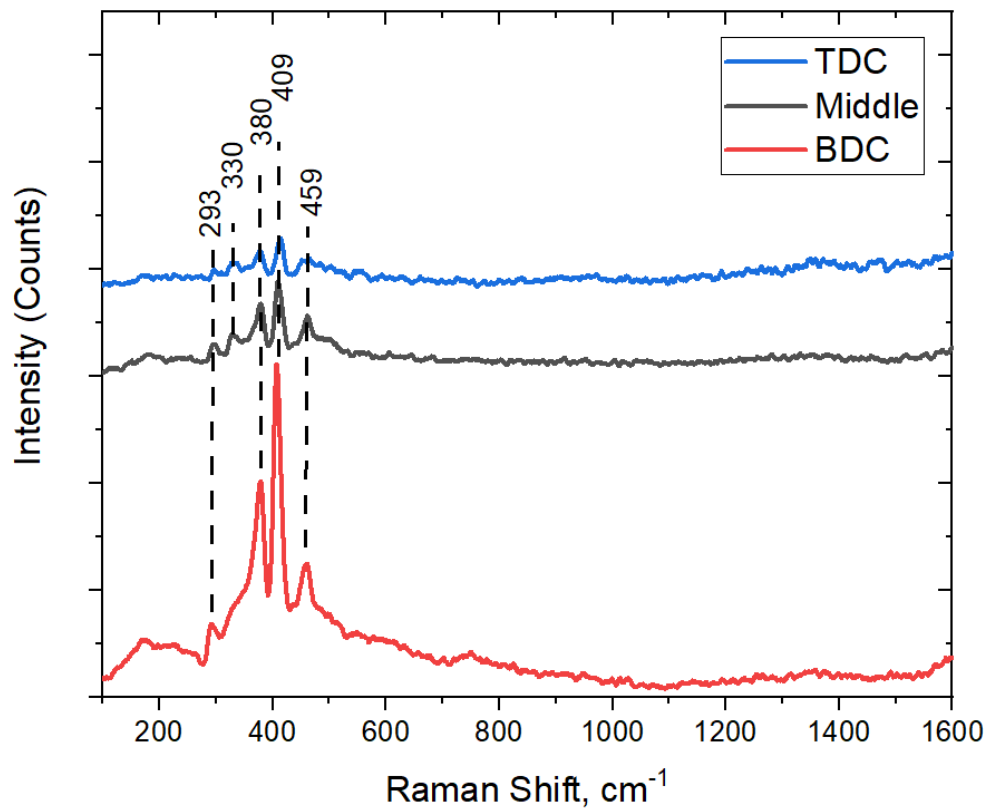
Figure 10 Single Raman spectra acquired with 3.3 mW laser power from the Liner 2 (FFO + 0.5 wt% MoDTC).

3.4 Pressure influence on MoS$_2$ tribofilm distribution

Figure 11 shows the Raman maps and histograms developed from two different regions on the BDC surface on the thrust and anti-thrust side of the Liner 2 (FF + 0.5 % MoDTC). The Raman mapping analysed areas and positions on the liner are shown in Figure 11 a). The optical images of the liner surface after the engine test are given in Figures 11 b) and e).

Raman map obtained from the thrust side of the liner is given in Figure 11 b) and shows that the MoS$_2$ area coverage is 72%. Conversely, the Raman map acquired from the anti-thrust side indicates a reduction of MoS$_2$ tribofilm area coverage of 53%. The observed coverage changes in the BDC area show that the tribofilm is non-uniformly distributed along the liner circumference. Furthermore, tribofilm coverage is seemingly dependant on the pressure experienced at the piston-liner tribocontact. Even more substantial differences are observed in Figures 11 c) and f). Therefore, fluctuations in histograms and cumulative intensity counts are expected.

Both simulation based [26] studies and experimental engine tests [26]–[28] demonstrated that the highest friction loss occurs during the expansion cycle when the piston contacts with the liner thrust side. Therefore, an increase of pressure on the thrust side of the engine would explain the higher MoS$_2$ area coverage, as tribocontact is subjected to a more severe boundary regime and more asperities are interacting at the contact.
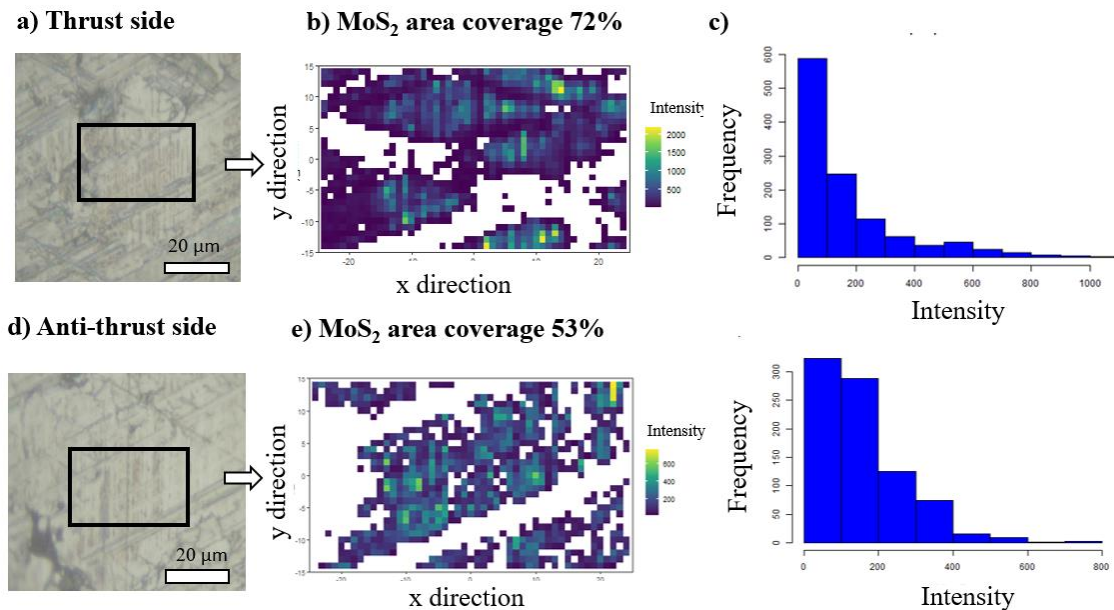

Figure 11 Liner 2 (tested with 0.5% MoDTC) analysis area from the BDC region on the thrust-side (a) and anti-thrust side (d). b), e) Raman maps acquired from thrust and anti-thrust sides, c) f) A$_{1g}$ peak intensity histogram.

3.5 Piston motion influence on the tribofilm distribution and layer thickness

According to the friction force results shown in Figure 8, the MoDTC effect on friction is the most prominent at the BDC region, where piston/liner contact operates predominantly in boundary lubrication conditions. Figure 12 shows Raman maps acquired from three different regions resembling variating lubrication conditions on the liner surface. For example, Figure 12 e) shows that the highest tribofilm coverage of 72% was reached at the BDC region, directly correlating with the increased friction reduction observed in Figure 8. On the other hand, the Raman map acquired from the middle of the liner shows a tribofilm area coverage reduction to 29% (Figure 12 c)), which is significantly smaller than BDC tribofilm coverage.

The variating piston dynamics could explain tribofilm differences along the stroke. The piston speed is the highest at the middle of the liner, and piston-liner contact operates more in mixed and hydrodynamic lubrication regimes. Therefore, a thicker lubricating film separates piston and liner; hence fewer asperities are at the tribocontact. Interestingly, friction force measurements (Figure 8) indicate that MoS_2 area coverage of 29% provides a friction reduction at the middle of the liner despite high piston speed. In this case, friction reduction at the middle of the liner could be attributed to the localised boundary lubrication regime due to the secondary piston motion.

Even more significant tribofilm area coverage reduction is observed at the TDC region (Figure 12 a)). The TDC MoS_2 area coverage is relatively low (9%) even though the boundary regime is expected at the piston reversal point. Tribofilm area coverage reduction at the TDC area corresponds with the lack of friction reduction at the TDC region during floating liner tests (Figure 8). Therefore, it is clear that MoDTC friction performance and MoS_2 tribofilm distribution are strongly affected by piston dynamics and contamination from the combustion chamber. In addition, TDC mapping results indicate that surface temperature and proximity to the combustion chamber cause a reduction of the MoS_2 area coverage as the TDC region is subjected to higher operating temperatures and contamination by the residuals of the combustion processes.
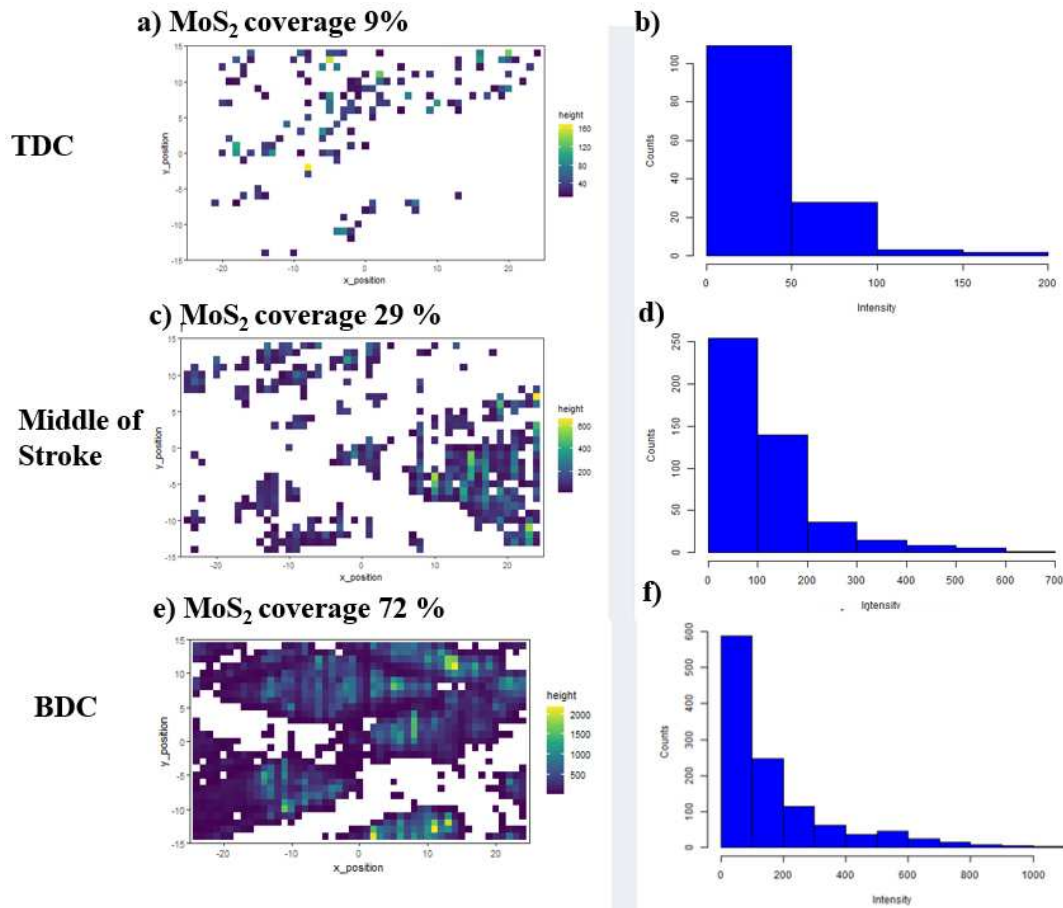
Figure 12 Raman maps acquired from the Liner 2 (FF + 0.5% MoDTC) presenting the A_{1g} peak intensity obtained from a) TDC area, c) middle of the liner, e) BDC area. The A_{1g} peak intensity histogram from b) TDC area, d) middle of the liner, and f) BDC area.

Figure 13 shows TEM micrographs from the TDC, middle of the liner, and BDC regions extracted from Liner 2 (0.5% MoDTC). Figure 13 b) and c) show that MoS_2 lamellar sheets are distributed parallel to the liner interface according to the piston sliding direction, which agrees with the previous TEM analysis on the MoS_2 tribofilms formed in benchtop tribometer tests [29], [30]. However, there is no publicly available TEM-based study on MoS_2 formation on engine components. Previous studies on the engine components tribochemistry were based on XPS [31] and Raman Microscopy [12].

Furthermore, no significant MoS_2 lamellar sheet formation was detected at the TDC region (Figure 13 a)). The majority of the tribofilm matrix in the TDC consists of an amorphous carbon-rich layer. Therefore, the absence of MoS_2 formation at the TDC region and domination of the amorphous carbon matrix could explain the lack of friction reduction in the TDC. Similar conclusions were made in Bewsher et al. [31] study on TDC region tribochemistry and Rai et al. [13] study on the MoS_2 lamellar structure formed in benchtop tribometers.

Tribofilm layer thickness in the TDC region varied from 30 nm to 120 nm. The middle of the liner exhibited a slightly thicker tribofilm thickness of 40 nm to 180 nm. Tribofilm thickness was slightly smaller in the BDC region and varied between 20 nm to 110 nm. Finally, no clear correlation between piston sliding speed and MoS_2 tribofilm thickness can be concluded, as the thickness varied significantly in each region. However,

this conclusion is expected since tribofilm thickness can not be solely correlated to the Lambda ratio as pressure, shear stresses, and local surface roughness play an important role [32].

a) Thickness at TDC - 30 nm to 120 nm
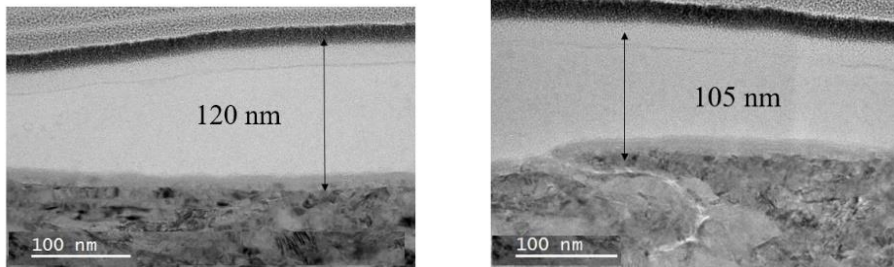
b) Thickness at the middle of liner - 40 nm to 180 nm
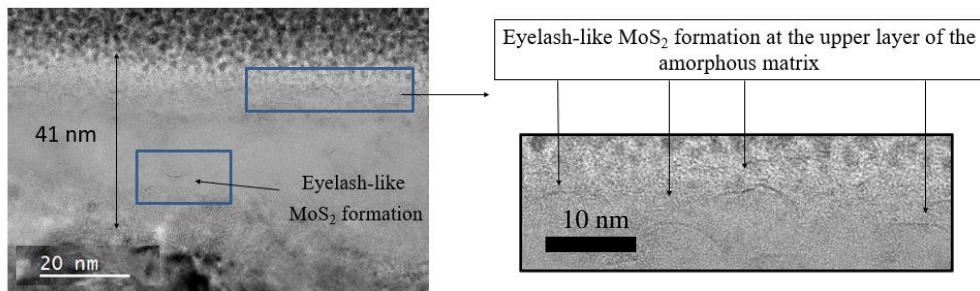
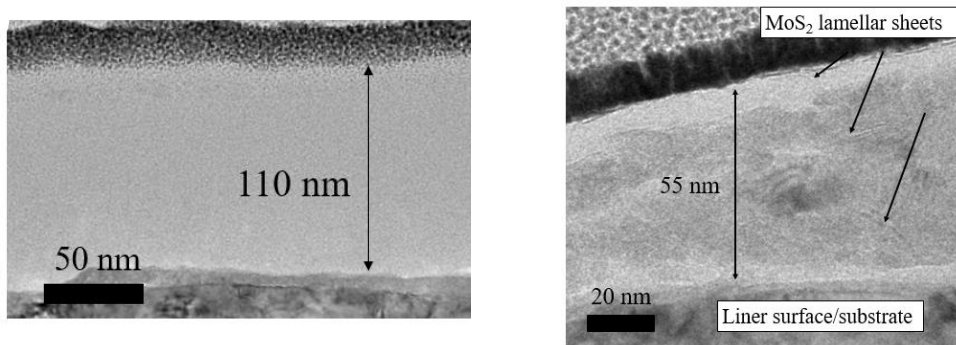**c) Thickness at BDC - 20 nm to 110 nm**

Figure 13 Tribofilm TEM micrographs extracted from the Liner 2 (0.5% MoDTC). a) TDC region, b) middle of liner, c) BDC region.

HAADF-STEM-EDX analysis was used to identify chemical element distribution across the tribofilm cross-section at TDC, middle and BDC regions. Figure 14 indicates that MoS_2 compounds are embedded into a Zn-rich tribofilm. Zn-rich tribofilm formation could be due to faster ZDDP decomposition in the tribocontact. Therefore, ZDDP decomposition products also function as a sulphur atom supply for the MoS_2 formation. Previous ZDDP and MoDTC tribochemistry studies [11], [29], [33] have shown that ZDDP presence in the fully-formulated lubricant improves MoS_2 formation, durability and adhesion to the substrate. Therefore, MoS_2 sheets tend to form on the upper layers of the tribofilm at the middle of the liner and BDC regions, which agrees with TEM images in Figures 13 b) and c). Additionally, some traces of molybdenum were detected in the TDC region as well.

In the middle of liner and BDC regions, calcium, sulphur, and zinc content are higher than in TDC region. According to the chemical component layout, MoS_2 sheet formation on top of anti-wear and detergent additives decomposition products. Therefore, the formation of protective films can be attributed to ZDDP additive and Ca-based detergent [34]. Additionally, oxygen and sulphur traces were found within the tribofilm matrix, which could be attributed to the decomposition of the fully formulated lubricant additives. However, it is challenging to address sulphur formation trends within the tribofilm matrix, as sulphur can be a ZDDP anti-wear additive decomposition product in the form of ZnS [35] and MoDTC breakdown to MoS_2.
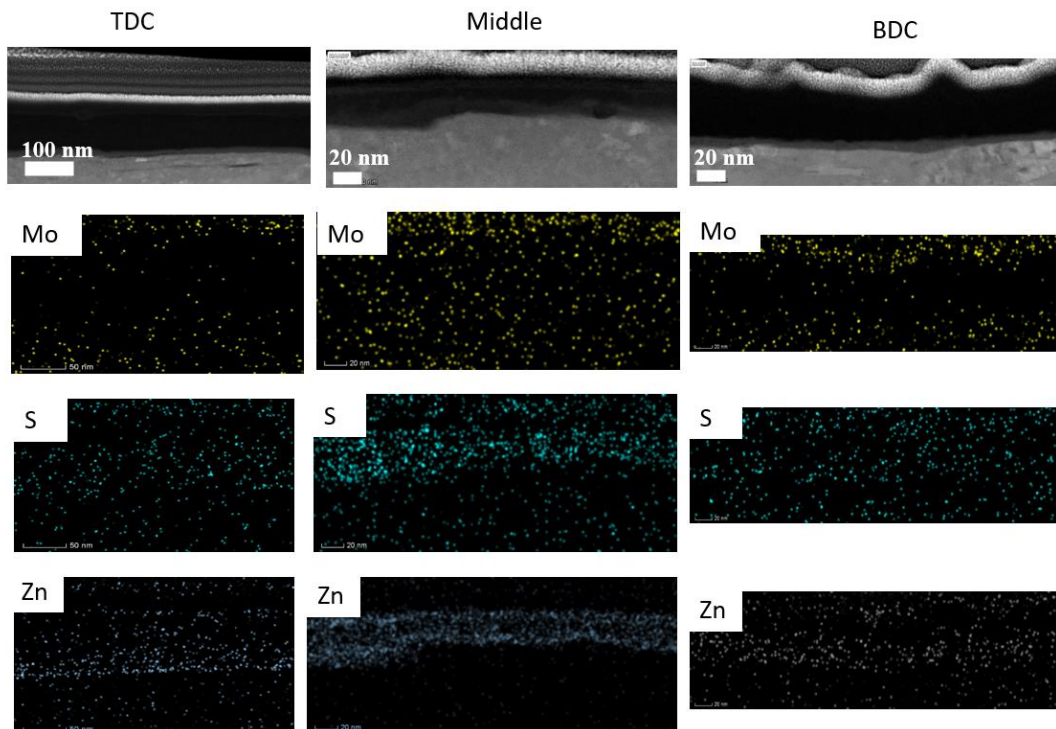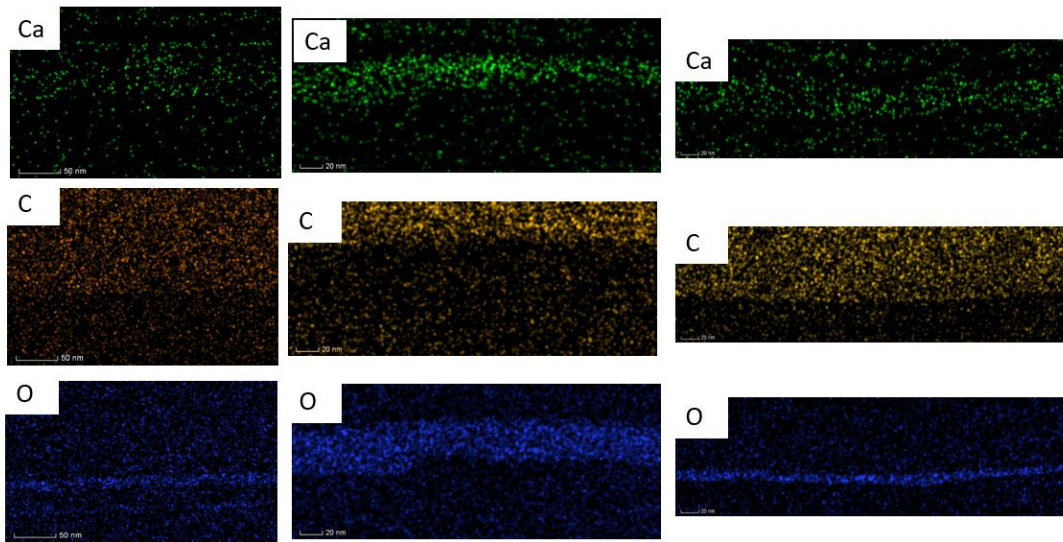
Figure 14 HAADF-STEM-EDX analysis on the TDC, middle of the liner and BDC tribofilm cross-sections extracted from the Liner 2 (0.5 % MoDTC).

3.6 MoDTC concentration influence on the tribofilm distribution on the liner

According to the friction force measurements in Figure 8, higher MoDTC concentration tests (0.7%, 0.5% and 0.3%) exhibited similar friction behaviour, whereas no friction reduction was observed in 0.1% MoDTC concentration tests. Therefore, it is important to evaluate the MoDTC concentration effect on MoS_2 tribofilm distribution as different friction behaviour was seen.

Figure 15 presents Raman maps acquired from the BDC region from all four tested liners. The analysed liner designation was previously given in Table 14, and Raman maps were obtained from the thrust side of each liner. Liner 1 (0.7% MoDTC) exhibited a highest area coverage of 95%, whereas lower concentration tests in 0.5% and 0.3% presented MoS_2 area coverage of 72% and 23%, respectively. Interestingly, despite the significant differences in the area coverage, all three liners had very similar friction reduction performance. As expected, Liner 4 (0.1% MoDTC) exhibited the smallest MoS_2 area coverage of 15%, and no friction reduction was observed during floating liner tests.
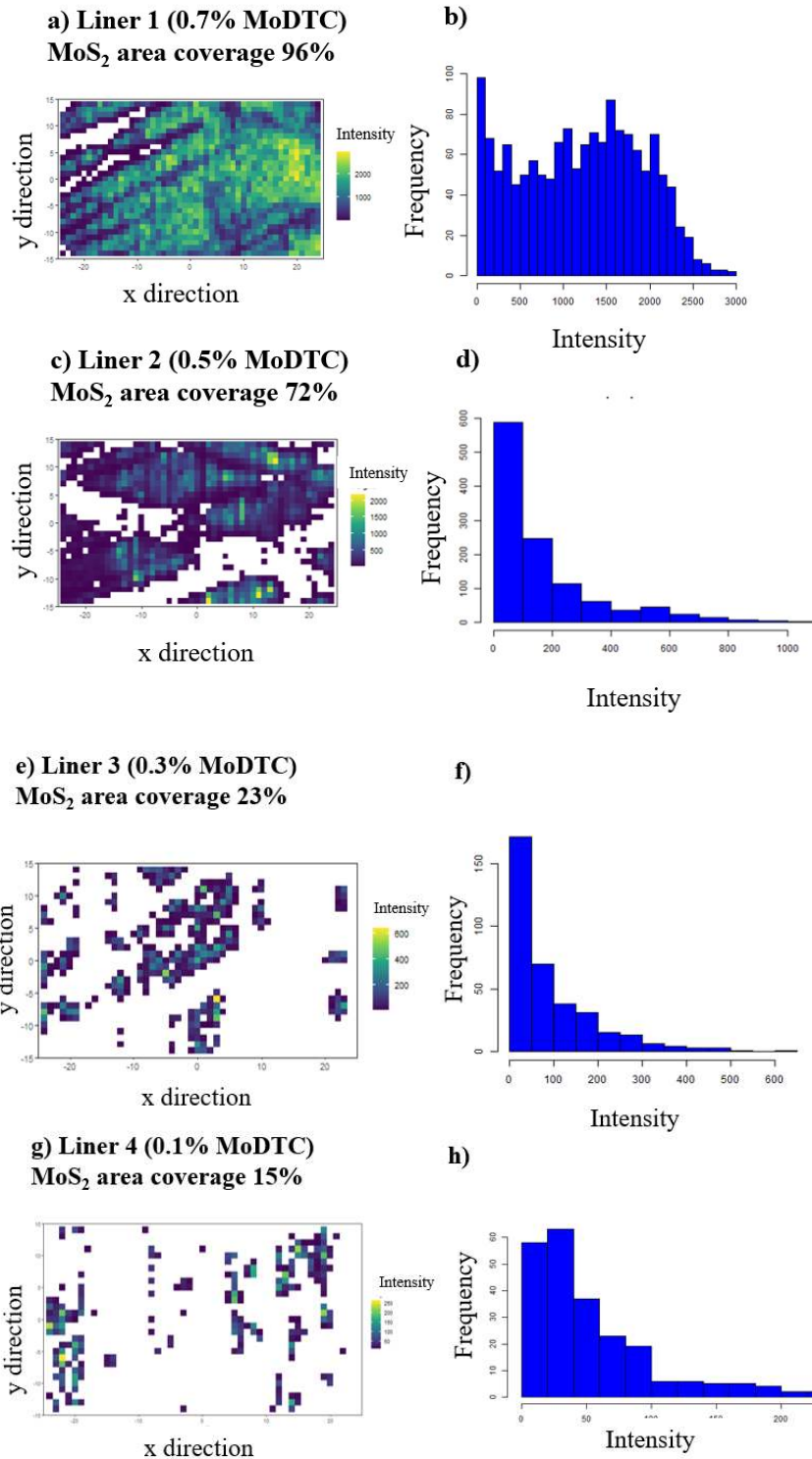
a) Liner 1 (0.7% MoDTC)
MoS₂ area coverage 96%

c) Liner 2 (0.5% MoDTC)
MoS₂ area coverage 72%

e) Liner 3 (0.3% MoDTC)
MoS₂ area coverage 23%

g) Liner 4 (0.1% MoDTC)
MoS₂ area coverage 15%

Figure 15 Ra...**Liner 1 tested in FF+0.**...**MoDTC, c), d) Liner 2 tested in FF+0.5% MoDTC, e), f) Liner 3 tested in FF+0.3% MoDTC, g) h) Liner 4 tested in FF+0.1% MoDTC.**

MoS₂ intensity distribution histograms (Figure 15 b), d), f), h)) are summarised in Figure 16. According to Figure 16, MoDTC concentration directly affects MoS₂ quantity generated during floating liner tests. Therefore, higher MoDTC concentration tests (0.7%, 0.5% and 0.3%) generally resulted in higher mean intensity, maximum intensity, and cumulative intensity values in Raman maps. Interestingly, the 0.1% MoDTC concentration test exhibited no friction reduction. However, according to the quantitative Raman map parameters shown in Figure

17, 0.1% and 0.3% MoDTC concentration tests presented a similar MoS_2 tribofilm formation. Therefore, it can be assumed that MoDTC concentration can influence the MoS_2 lamellar structure and layout across the tribofilm, which is not evaluated by Raman Microscopy mapping.
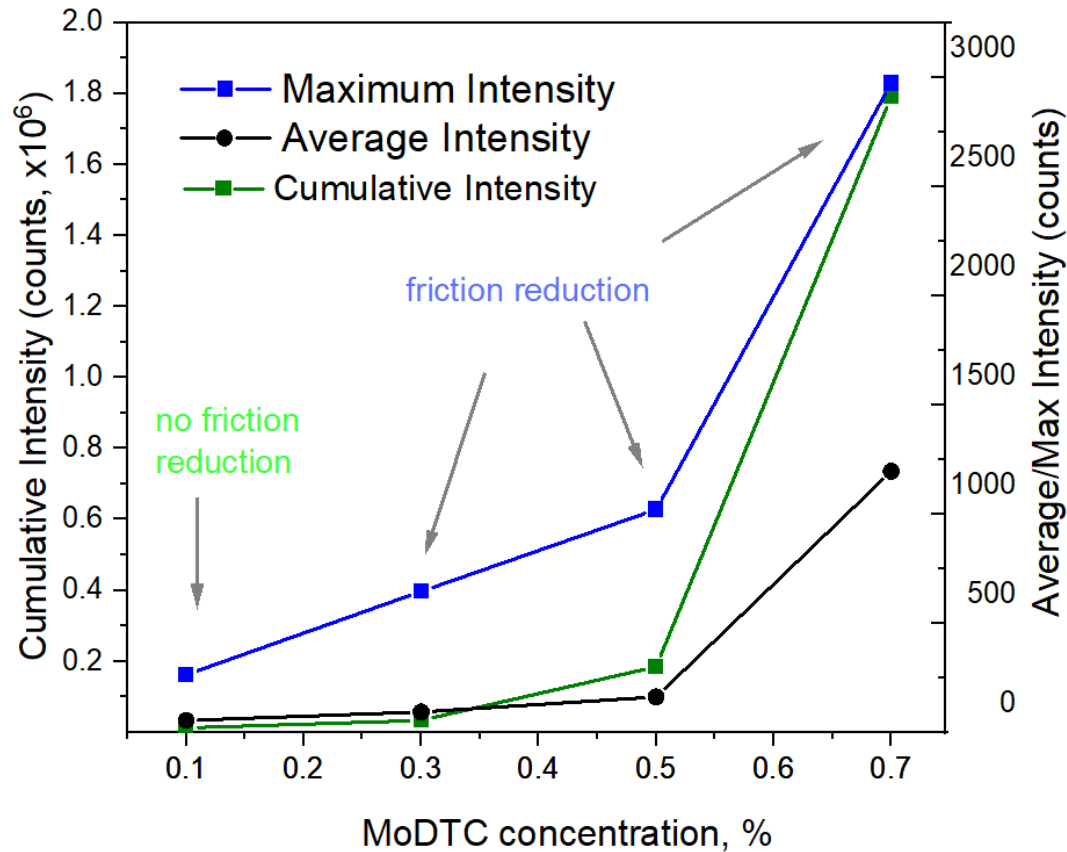

Figure 16 A_{1g} peak intensity quantification according to the Raman maps acquired from the BDC region. Raman maps were obtained from the thrust side of the Liners 1, 2, 3 and 4, tested in 0.7%, 0.5%, 0.3% and 0.1% MoDTC concentrations, respectively.

The differences in friction behaviour observed during floating liner tests can be related to different tribofilm structures as a result of variating MoDTC concentrations in the oil. Figure 17 shows the MoDTC concentration effect on MoS_2 tribofilm formation on the liner. Figure 17 a) shows that tribofilm generated on Liner 1 (0.7% MoDTC) exhibit distinct MoS_2 lamellar sheets compared to tribofilm formed on Liner 2 (0.5% MoDTC). There was no clear correlation between Liner 1 and Liner 2 tribofilm thickness, as cross-section measurements varied greatly from 35 nm to 120 nm.

Tribofilm formed in smaller MoDTC concentration conditions presents fewer MoS_2 lamellar sheets. Therefore, it can be assumed that higher MoDTC concentration tests are prone to build more MoS_2 lamellar sheets within the amorphous tribofilm matrix and contribute to higher friction reduction due to increased shearing between the lamellar sheets. However, this observation is conditioned to the limitations of the FIB/TEM system analysis. It is important to consider that FIB/TEM analysis area is small, which sometimes are not statistically

representative of a larger area, such as the liner surface. Additionally, according to the previous research conducted on the MoS_2 sheets 2D coverage, it is clear that MoS2 sheet distribution varies depending on the local roughness and topography features [11], [36]. Thus, MoS_2 sheet concentration can vary greatly in different FIB extracted samples. However, to minimise the uncertainties in the measurements, the FIB extraction location and procedure was kept constant for all liners. Additionally, 2 to 4 FIB cross-section samples were extracted from the same area, which deemed to be representable.

a) Liner 1 (0.7% MoDTC), BDC region
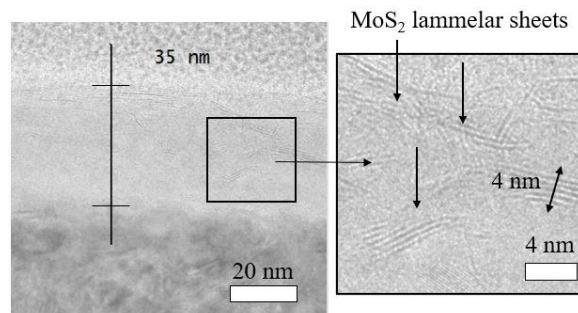
b) Liner 2, (0.5% MoDTC), BDC region
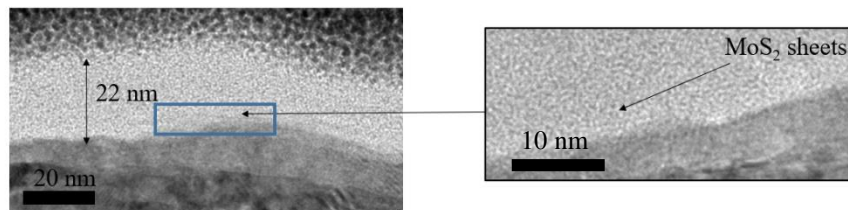
Figure 17 MoS₂ lamellar sheet distribution in the tribofilm cross-section from a) Liner 1 (0.7% MoDTC), b) Liner 2 (0.5% MoDTC).

Figure 18 shows HAADF-STEM-EDX mapping in different MoDTC concentration tests. Generally, chemical element mapping indicates that MoS_2 lamellar sheets are embedded into carbon and oxygen-rich matrix in both MoDTC concentration tests. Moreover, as expected, higher MoDTC concentration tests exhibit a more distinct molybdenum and sulphur particle distribution within the amorphous tribofilm matrix (Figure 18 a)). Interestingly, higher MoDTC concentration tests indicate smaller carbon content compared to the 0.5% MoDTC concentration test, the carbon scale is kept constant in all scans for representative purposes And generally, fully formulated oil additives distributed more uniformly on Liner 1 (0.7% MoDTC) than Liner 2 (0.5% MoDTC). Additionally, the dominant traces of calcium, zinc and sulphur were detected for both concentrations.

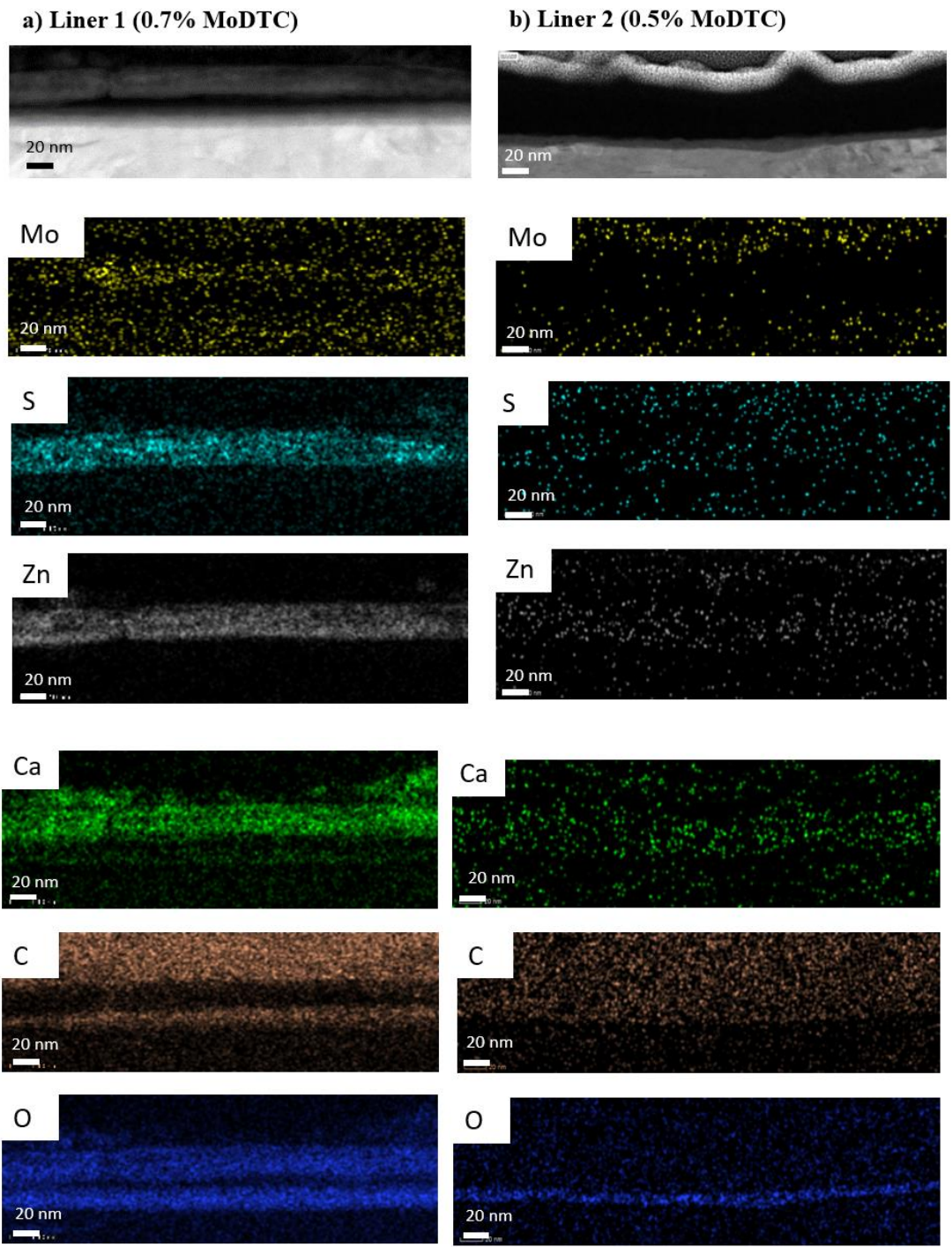**a) Liner 1 (0.7% MoDTC)**　　**b) Liner 2 (0.5% MoDTC)**

Figure 18 HAADF-STEM-EDX analysis on the tribofilm cross-sections from BDC region on a) Liner 1 (0.7% MoDTC) and b) Liner 2 (0.5 % MoDTC).

4 DISCUSSION

4.1 MoS$_2$ tribofilm formation in piston-liner tribocontact

The piston sliding speed is one of the parameters that define the fluid film thickness in the piston-cylinder contact and, consequently, the extent of asperity contacts and boundary lubrication severity. Considering that the formation of MoS$_2$ sheets is accelerated by the severity of the contact at surface asperities [11], the boundary regime at piston reversal points is expected to result in a higher rate of MoS$_2$ tribofilm formation/removal and wear. The tribofilm coverage is also non-uniform along the liner circumference since the highest MoS$_2$ coverage is observed on the thrust side of the engine.

It is worth noticing that extreme pressures can also cause removing honing grooves and abrasive wear presented in the SEM image in Figure 9. Corresponding Raman maps provided in Figure 12 reveal that the highest MoS$_2$ tribofilm coverage is observed on the worn-out areas at the BDC position, indicating severe contact pressure at the asperities. Furthermore, both simulation-based [26] studies and experimental engine tests [26]–[28] demonstrated that the highest friction loss occurs during the expansion cycle when the piston skirt collides with the cylinder liner thrust side. As a result, the lateral force between cylinder liner and piston skirt reaches the maximum, reducing the oil film thickness and increasing the contact between asperities.

A simulation-based study conducted by Meng et al. [26] proposed an oil transportation model on the thrust side of the cylinder. Their simulation model concluded that the BDC region operates under sufficient lubrication conditions. When the piston drags upwards, and oil film thickness reduces significantly at the TDC. Their research concluded that a severe oil thinning is experienced at the expansion stroke, which causes a piston skirt and cylinder liner collision [26].

The proposed oil transportation model could explain the observed MoDTC decomposition and MoS$_2$ formation trends in piston-liner contact. Since the piston ring operates under sufficient lubrication conditions at the BDC region, a constant supply of MoDTC at the contact increases the MoS$_2$ formation rate leading to the higher MoS$_2$ coverage. When the piston drags upwards (shown in Figure 19), MoDTC supply at the tribocontact is reduced. Therefore, it can be assumed that MoS$_2$ area coverage reduces due to low lubricant supply at the TDC [26]. Due to lubricant starvation conditions and high operating temperatures at the TDC, the MoS$_2$ formation rate is lower. Additionally, the relation between MoDTC friction reduction capacity, concentration in the base oil and testing temperature, were previously observed by Graham et al. [37]. Hence, significantly smaller MoS$_2$ area coverage at the TDC region corresponds with a lack of friction reduction.
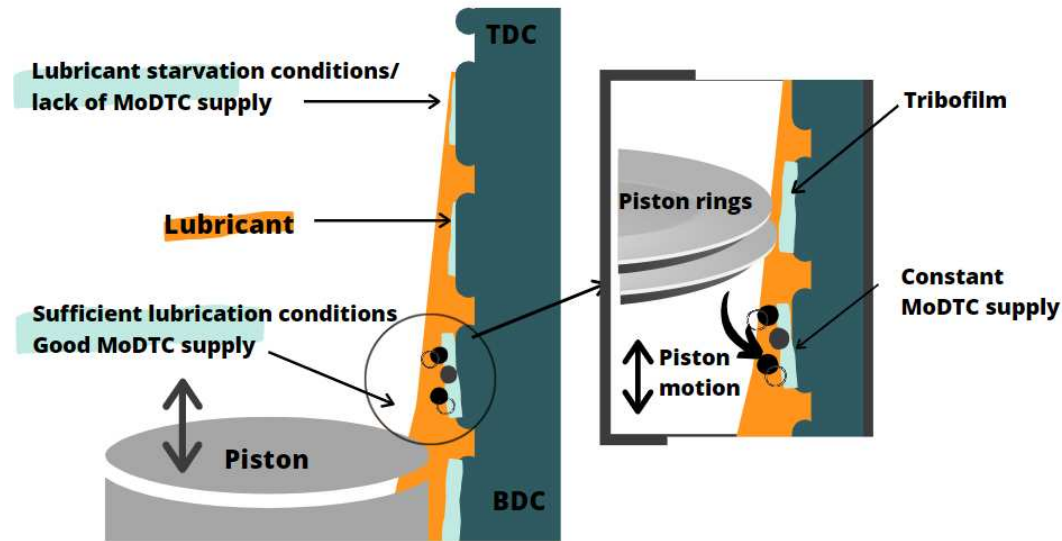
Figure 19 Lubricant transportation model during the engine cycle

It is essential to consider that even though piston speed defines the lubrication regime in the piston-liner contact surface temperatures, the unburnt fuel, sludge production, gas pressure, and the combustion process can significantly influence the effectiveness of the lubricant. For example, the combustion influence on the MoS_2 tribofilm formation is evident in Figure 12, as a very small MoS_2 coverage was detected on the TDC area.

4.2 MoDTC concentration effect on MoS_2 coverage and friction force

Friction force measurements in different MoDTC concentrations (Figure 20 c)) reveal that MoDTC in the lubricant had the most substantial impact on the piston reversal point at the BDC area during the engine cycle where the boundary regime is expected. However, no MoDTC effect was observed at the TDC area, regardless of the MoDTC concentration in the lubricant.

Figure 20 a) shows a friction force reduction during the compression stroke as the piston moves from BDC to TDC. Figure 20 b) shows averaging MoS_2 area coverage on the liner at thrust and anti-thrust sides. The MoS_2 area coverage was acquired at equally separated intervals from BDC to TDC. According to Figure 20, MoS_2 tribofilm coverage decreases exponentially from the BDC area to the TDC area, corresponding with friction force reduction in the liner during the engine test. Based on studies conducted on the benchtop tribometers, this observation is expected when a neat correlation between MoS_2 coverage and coefficient of friction was observed in tests in base oils conducted by Xu et al. [11].

The highest friction force reduction during combustion stroke was achieved with 0.7%, 0.5% and 0.3% MoDTC tests. Furthermore, a 0.1% MoDTC test exhibited higher friction, similar to the fully formulated oil without added MoDTC. The highest friction reduction was observed in the BDC, corresponding with the richest MoS_2 coverage regions on the cylinder shown in Figure 20 b). Figure 20 b) shows that MoDTC concentration reduction to 0.3% and 0.1% substantially decreased MoS_2 coverage to 25 % and 15 %, respectively. The reduction of MoS_2 coverage would explain the high friction observed in the 0.1% MoDTC tests. However, 0.3% MoDTC

tests maintained the friction reduction despite the MoS_2 area coverage decrease.

a)

b)

c)
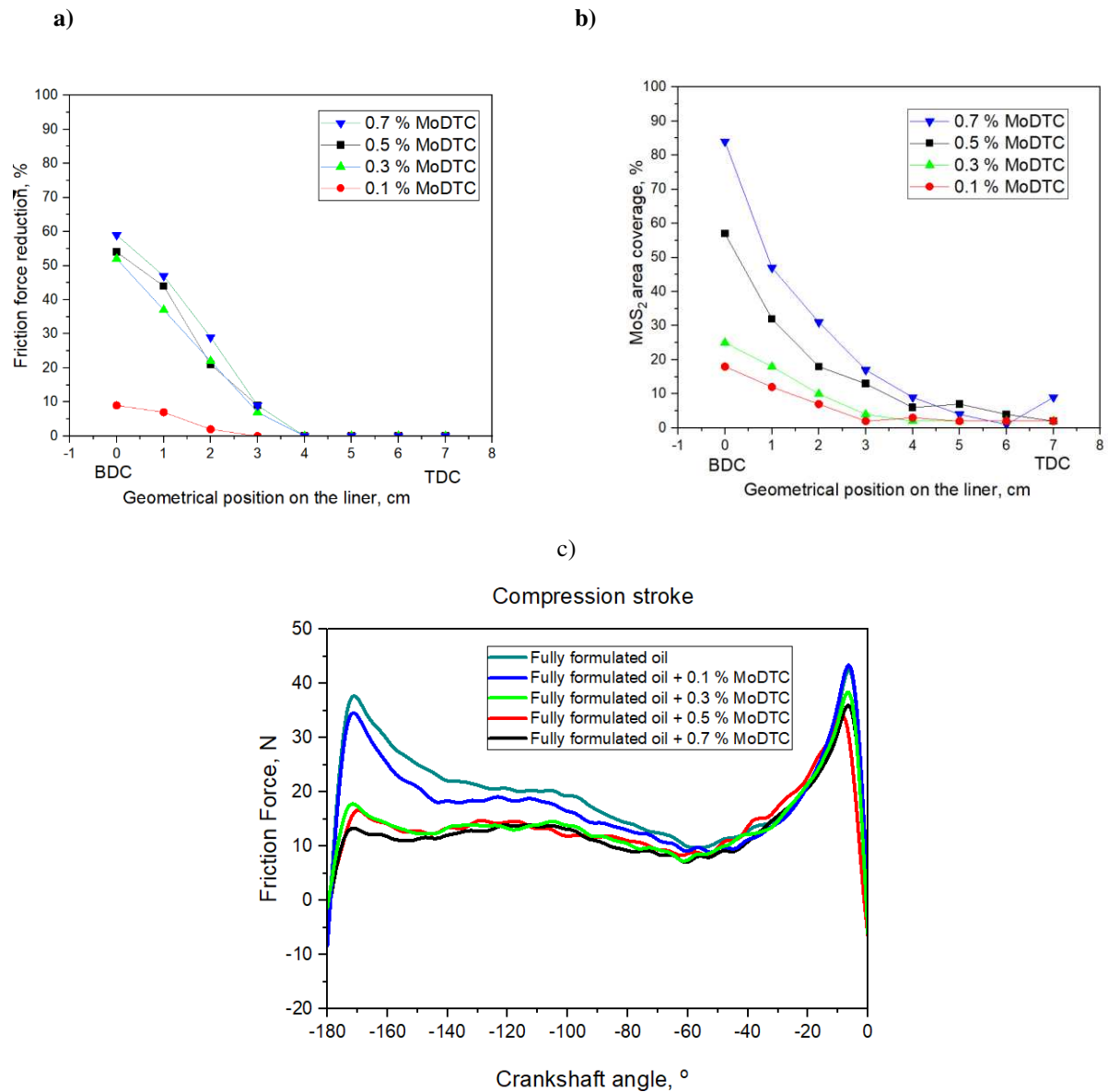
Figure 20 a) MoDTC concentration effect on the friction force reduction during combustion cycle in floating liner system b) Resulting MoS_2 area coverage distribution from BDC to TDC in variating MoDTC concentrations, c)) Comparison of the MoDTC concentration influence on the measured friction force in the liner during compression stroke.

Interestingly, a significant amount of MoS_2 formation is observed in the middle of the liner, indicating potential MoDTC effectiveness during the entire engine cycle. This is the first time that MoS_2 tribofilm formation is reported in the mid-stroke area. Wear appearance in the middle of the liner (Figure 9 b)) indicates possible contact at the asperities due to a possible secondary motion of the piston skirt. Generally, the clearance between piston-cylinder and connecting rod components and the dynamic contact forces during the four-stroke engine cycle create

lateral movements in the piston, causing the piston to tilt [26], [38], [39]. The following section discusses the piston secondary motion effect on piston/liner tribochemistry.

4.3 Piston secondary motion effect on MoS$_2$ tribofilm distribution

Experimentally-based tribology studies [21], [31], [40] mainly investigate the piston/liner contact in the ideal piston sliding conditions (one degree of freedom), considering only the primary piston sliding motion from TDC to BDC. However, in real life, the piston operates in six degrees of freedom, including secondary motion of the piston, piston tilt and ring rotation. According to Raman microscopy results given in Figure 12, it is clear that MoDTC influences friction performance across the whole cylinder liner due to piston secondary motion. Hence, the MoS$_2$ tribofilm formation in the middle of the liner contradicts the previous beliefs that the MoDTC effect is visible only on the piston reversal points at TDC and BDC [12].

Numerical simulation models on piston secondary motion proposed by Murakami et al. [39], Meng et al. [26] and Forero et al. [38] concluded that piston dynamics are complex. Meng et al. [26] oil transportation model provided evidence that elastohydrodynamic, mixed and boundary lubrication co-occurs in the middle of the cylinder. Combined experimental and numerical studies prove that boundary lubrication and resulting MoS$_2$ tribofilm formation are defined by oil transportation between piston and cylinder liner. Oil transportation and distribution are strongly affected by lubricating film amount as defined Lambda ratio, piston side pressure and sliding speed during piston skirt collision with cylinder liner. Therefore, a piston dynamics mechanism described below explains MoS$_2$ tribofilm formation at the middle of the cylinder.

Figure 21 shows a simplified scheme of the piston movement occurring in the cylinder. The chemical energy released in the combustion chamber transfers into kinetic energy as the piston pushes down from TDC to BDC. The movement is passed from piston head to piston pin and connecting rod. Connecting rod transports the motion to the crankshaft rotation. As a result, connecting rod axial is not always perpendicular to the piston head. Therefore connecting rod angle causes a lateral motion and piston skirt collision with the cylinder liner, also known as piston secondary motion. Hence, piston movement is determined by the pressure load, connecting-rod angle and restricted by the cylinder liner, creating boundary lubrication conditions.
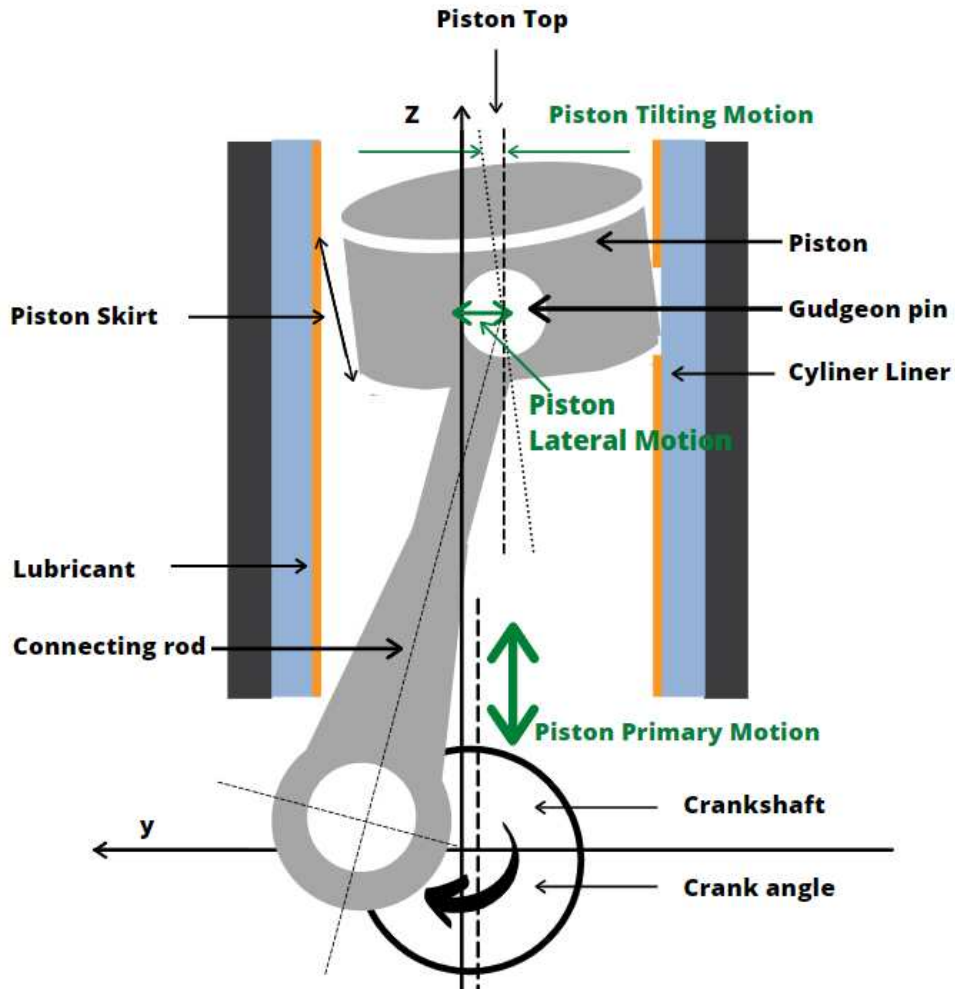
Figure 21 Schematics of piston skirt secondary contact with the liner.

4.4 Fully formulated lubricant chemistry effect on MoS$_2$ tribofilm chemical composition

Generally, the tribofilm consists of carbon and oxygen-rich matrix with MoS$_2$ lamellar sheets embedded into zinc and calcium compounds. A similar tribofilm layer arrangement has been previously reported when testing MoDTC with PAO base oils [13] and MoDTC/ZDDP with PAO base oils [11]; however, there is a lack of information on MoS$_2$ tribofilm formation in fully formulated low viscosity lubricants.

TEM images, shown in Figures 18 and 19, indicate that MoS$_2$ tribofilm formation varies depending on the engine operating conditions. Furthermore, tribofilm structure changes significantly depending on the liner region. MoS$_2$ lamellar sheets are distributed parallel to the cylinder liner interface according to the piston sliding direction, which agrees with the TEM analysis on the MoS$_2$ tribofilms formed in tribometer tests [29], [41]. These are new results on MoS$_2$ tribofilm formation since there is no publicly available TEM analysis on MoS$_2$ formation on engine components. Previous studies on the engine components were based on XPS [42] and Raman Microscopy [12].

The majority of the tribofilm matrix in the TDC centre consists of carbon-rich compounds. HAADF measurements in Figure 14 indicate that carbon compounds cover the upper layer of the tribofilm, which is in

good agreement with fired engine tests conducted by Bewsher et al. [31]. In their study [31], a carbon formation was attributed to the incomplete combustion. Additionally, carbon reduction can be attributed to the lower surface temperatures at BDC compared to the high operating temperatures of TDC. Therefore, the absence of MoS_2 formation at the TDC region and domination of the amorphous carbon matrix could explain the lack of friction reduction in the TDC. Moreover, according to the TEM images provided by Rai *et al.* [13], the lack of MoS_2 lamellar sheet structure in the tribofilm layer resulted in high friction.

Additionally, oxygen and sulphur traces were found within the tribofilm matrix, which could be attributed to the decomposition of the fully formulated lubricant additives. However, it is challenging to address sulphur formation trends within the tribofilm matrix, as sulphur can be a ZDDP anti-wear additive decomposition product in the form of ZnS [43] and MoDTC breakdown to MoS_2.

Furthermore, MoS_2 lamellar sheets analysed in this study are formed on the upper layer of the tribofilm, parallel to the shearing plane. Interestingly, in the middle of the liner and BDC regions, MoS_2 sheets form on the upper layers of the tribofilm, despite the higher Lambda ratio conditions, reducing contact between asperities. Oxygen, calcium, sulphur, and zinc layer concentration increases, forming at the cylinder liner interface. MoS_2 sheet formation on top of anti-wear and detergent compounds can be attributed to the faster breakdown of ZDDP and Ca-based detergent [34] and the formation of the protective films. Additionally, no clear correlation between piston sliding speed and MoS_2 tribofilm thickness can be concluded, as the thickness varied significantly in each region.

Moreover, it is essential to consider the variating lubrication regimes during the engine cycle and lubricant supply at the tribocontact. Meng et al. [26] observed that when the piston is at BDC, there is a sufficient lubricant on the cylinder liner to start forming protective films. However, piston drags upwards, and oil film thickness reduces significantly at the TDC, reducing lubricant supply. Therefore, it can be assumed that BDC and middle cylinder have more compliant lubrication conditions for fully formulated lubricant adsorption and decomposition, without a significant interference of the combustion effect, resulting in higher friction reduction and MoDTC effectiveness.

5 CONCLUSIONS

In this study, molybdenum-containing low viscosity fully formulated lubricants are tested according to the floating liner measurement method. In addition, Raman microscopy was employed to analyse the piston stroke influence on the liner during the engine cycle. This study confirms for the first time that MoS_2 tribofilm spatial distribution impacts the friction force reduction in the piston-liner tribological contact in a fired engine. Other conclusions are:

1. Floating liner measurements from fired engine tests reveal that MoDTC in the lubricant had the most substantial impact on the piston reversal point at the BDC area where the boundary regime is expected. However, no MoDTC effect was observed at the TDC area, regardless of the MoDTC concentration in the lubricant.

2. MoDTC concentration directly affects MoS_2 quantity generated during floating liner tests. Therefore, higher MoDTC concentration tests (0.7%, 0.5% and 0.3%) generally resulted in higher mean intensity, maximum intensity, and cumulative intensity values in Raman maps.

3. MoS_2 tribofilm coverage is the highest at the ring reversal point at the BDC region and can grow to 95% area coverage depending on whether it is formed on the thrust or anti-trust side of the engine. Generally, liner thrust-side exhibited higher MoS_2 area coverage.

4. Despite the highest piston speed and dominant mixed and hydrodynamic lubrication, MoS_2 formation was detected in the middle part of the stroke. MoS_2 formation in the middle of the liner could be attributed to the piston secondary motion effect, which induces a local boundary/mix lubrication regime between the skirt and the liner in the midstroke area.

5. A carbon-rich tribofilm matrix is formed on the TDC area, which is ineffective in reducing friction and is strongly influenced by the high surface temperatures, resulting in thermal oil and combustion contamination.

REFERENCES

[1]   European Environment Agency (EEA), "Greenhouse gas emissions from transport in Europe," 2018. [Online]. Available: https://www.eea.europa.eu/data-and-maps/indicators/transport-emissions-of-greenhouse-gases/transport-emissions-of-greenhouse-gases-11.

[2]   U.S. Environmental Protection Agency (EPA), "Sources of Greenhouse Gas Emissions," 2017. [Online]. Available: https://www.epa.gov/ghgemissions/sources-greenhouse-gas-emissions.

[3]   K. Holmberg, P. Andersson, and A. Erdemir, "Global energy consumption due to friction in passenger cars," *Tribol. Int.*, vol. 47, pp. 221–234, 2012, doi: 10.1016/j.triboint.2011.11.022.

[4]   K. Holmberg and A. Erdemir, "The impact of tribology on energy use and CO2 emission globally and in combustion engine and electric cars," *Tribol. Int.*, vol. 135, pp. 389–396, Jul. 2019, doi: 10.1016/J.TRIBOINT.2019.03.024.

[5]   K. Holmberg, P. Andersson, N. O. Nylund, K. Mäkelä, and A. Erdemir, "Global energy consumption due to friction in trucks and buses," *Tribol. Int.*, vol. 78, pp. 94–114, 2014, doi: 10.1016/j.triboint.2014.05.004.

[6]   J. Heywood, *Internal Combustion Engine Fundamentals*. McGraw-Hill Education, 1988.

[7]   Y. Hamid, A. Usman, S. K. Afaq, and C. W. Park, "Numeric based low viscosity adiabatic thermo-tribological performance analysis of piston-skirt liner system lubrication at high engine speed," *Tribol. Int.*, vol. 126, no. March, pp. 166–176, 2018, doi: 10.1016/j.triboint.2018.05.022.

[8]   D. E. Richardson, "Review of Power Cylinder Friction for Diesel Engines," *J. Eng. Gas Turbines Power*, vol. 122, no. 4, pp. 506–519, 2000, doi: 10.1115/1.1290592.

[9]   D. N. Khaemba, A. Neville, and A. Morina, "New insights on the decomposition mechanism of Molybdenum DialkyldiThioCarbamate (MoDTC): a Raman spectroscopic study," *RSC Adv.*, vol. 6, no. 45, pp. 38637–38646, 2016, doi: 10.1039/C6RA00652C.

[10]   D. N. Khaemba, A. Neville, and A. Morina, "A methodology for Raman characterisation of MoDTC tribofilms and its application in investigating the influence of surface chemistry on friction performance of MoDTC lubricants," *Tribol. Lett.*, vol. 59, no. 3, pp. 1–17, 2015, doi: 10.1007/s11249-015-0566-6.

[11]   D. Xu, C. Wang, C. Espejo, J. Wang, A. Neville, and A. Morina, "Understanding the Friction Reduction Mechanism Based on Molybdenum Disulfide Tribofilm Formation and Removal," *Langmuir*, vol. 34, no. 45, pp. 13523–13533, 2018, doi: 10.1021/acs.langmuir.8b02329.

[12]   C. Espejo, C. Wang, B. Thiébaut, C. Charrin, A. Neville, and A. Morina, "The role of MoDTC tribochemistry in engine tribology performance. A Raman microscopy investigation," *Tribol. Int.*, vol. 150, no. April, 2020, doi: 10.1016/j.triboint.2020.106366.

[13]   A. M. Yugal Rai, Anne Neville, "Transient processes of MoS2 tribofilm formation under boundary lubrication," *Lubr. Sci.*, vol. 28, no. 6, pp. 449–471, 2016, doi: 10.1002/ls.

[14]   J. Edtmayer, S. Lösch, H. Hick, and S. Walch, "Comparative study on the friction behaviour of piston/bore interface technologies," *Automot. Engine Technol.*, vol. 4, no. 3–4, pp. 101–109, 2019, doi: 10.1007/s41104-019-00045-x.

[15]   E. Winklhofer, S. Loesch, and S. Satschen, "High precision piston to liner friction measurement," no. November, p. 20165350, 2016.

[16]   E. Winklhofer, S. Loesch, S. Satschen, and B. Thonhauser, "Reduction of Friction Losses by Means of Cylinder Liner Offset in a Floating Liner Single Cylinder Engine," *Int. J. Automot. Eng.*, vol. 9, no. 4, pp. 304–309, 2018, doi: 10.20485/jsaeijae.9.4_304.

[17]   D. Uy, S. J. Simko, R. O. Carter, R. K. Jensen, and A. K. Gangopadhyay, "Characterization of anti-wear films formed from fresh and aged engine oils," *Wear*, vol. 263, no. 7-12 SPEC. ISS., pp. 1165–1174, 2007, doi: 10.1016/j.wear.2006.12.026.

[18]   M. K. A. Ali, H. Xianjun, L. Mai, C. Qingping, R. F. Turkson, and C. Bicheng, "Improving the tribological characteristics of piston ring assembly in automotive engines using Al2O3 and TiO2 nanomaterials as nano-lubricant additives," *Tribol. Int.*, vol. 103, pp. 540–554, 2016, doi: 10.1016/j.triboint.2016.08.011.

[19]   P. Papadopoulos, M. Priest, and W. M. Rainforth, "Investigation of fundamental wear mechanisms at the piston ring and cylinder wall interface in internal combustion engines," *Proc. Inst. Mech. Eng. Part J J. Eng. Tribol.*, vol. 221, no. 3, pp. 333–343, 2007, doi: 10.1243/13506501JET254.

[20]   L. I. Farfan-Cabrera, E. A. Gallardo-Hernández, J. Pérez-González, B. M. Marín-Santibáñez, and R. Lewis, "Effects of Jatropha lubricant thermo-oxidation on the tribological behaviour of engine cylinder liners as measured by a reciprocating friction test," *Wear*, vol. 426–427, no. August 2018, pp. 910–918, 2019, doi: 10.1016/j.wear.2019.02.028.

[21]   Y. Peng, Y. Xu, J. Geng, K. D. Dearn, and X. Hu, "Tribological assessment of coated piston ring-cylinder liner contacts under bio-oil lubricated conditions," *Tribol. Int.*, vol. 107, no. December 2016, pp. 283–293, 2017, doi: 10.1016/j.triboint.2016.12.004.

[22]   D. dos Santos Filho, A. P. Tschiptschin, and H. Goldenstein, "Effects of ethanol content on cast iron cylinder wear in a flex-fuel internal combustion engine–A case study," *Wear*, vol. 406–407, no. April, pp. 105–117, 2018, doi: 10.1016/j.wear.2018.04.003.

[23]   Z. Dimkovski, C. Anderberg, R. Ohlsson, and B. G. Rosén, "Characterisation of worn cylinder liner surfaces by segmentation of honing and wear scratches," *Wear*, vol. 271, no. 3–4, pp. 548–552, 2011, doi: 10.1016/j.wear.2010.04.024.

[24]   J. M. Chen and C. S. Wang, "Second order Raman spectrum of MoS2," *Solid State Commun.*, vol. 14, no. 9, pp. 857–860, 1974, doi: 10.1016/0038-1098(74)90150-1.

[25]   T. J. Wieting, "Long-wavelength lattice vibrations of MoS2 and GaSe," *Solid State Commun.*, vol. 12, no. 9, pp. 931–935, 1973, doi: 10.1016/0038-1098(73)90111-7.

[26]   Z. Meng, S. Ahling, and T. Tian, "Modeling of oil transport between piston skirt and cylinder liner in internal combustion engines," *SAE Tech. Pap.*, vol. 2019-April, no. April, pp. 1–11, 2019, doi: 10.4271/2019-01-0590.

[27]   P. P. Totaro, Z. Westerfield, and T. Tian, "Introducing a New Piston Skirt Profile to Reduce Engine Friction," *SAE Tech. Pap.*, 2016, doi: 10.4271/2016-01-1046.

[28]   Z. Westerfield, P. Totaro, D. Kim, and T. Tian, "An Experimental Study of Piston Skirt Roughness and Profiles on Piston Friction Using the Floating Liner Engine," *SAE Tech. Pap.*, 2016, doi: 10.4271/2016-01-1043.

[29]   J. M. Martin, C. Grossiord, K. Varlot, B. Vacher, and J. Igarashi, "Synergistic effects in binary systems of lubricant additives: A chemical hardness approach," *Tribol. Lett.*, vol. 8, no. 4, pp. 193–201, 2000, doi: 10.1023/A:1019147520893.

[30]   M. De Feo *et al.*, "Ageing impact on tribological properties of MoDTC-containing base oil," *Tribol. Int.*, vol. 92, pp. 126–135, 2015, doi: 10.1016/j.triboint.2015.04.014.

[31]   S. R. Bewsher, M. Leighton, M. Mohammadpour, H. Rahnejat, G. Offner, and O. Knaus, "Boundary friction characterisation of a used cylinder liner subject to fired engine conditions and surface deposition," *Tribol. Int.*, vol. 131, no. September 2018, pp. 424–437, 2019, doi: 10.1016/j.triboint.2018.11.005.

[32]   J. Zhang and H. Spikes, "On the Mechanism of ZDDP Antiwear Film Formation," *Tribol. Lett.*, vol. 63, no. 2, pp. 1–15, 2016, doi: 10.1007/s11249-016-0706-7.

[33]   A. Morina and A. Neville, "Understanding the composition and low friction tribofilm formation/removal in boundary lubrication," *Tribol. Int.*, vol. 40, no. 10-12 SPEC. ISS., pp. 1696–1704, 2007, doi: 10.1016/j.triboint.2007.02.001.

[34]   T. Kubo, S. Fujiwara, H. Nanao, I. Minami, and S. Mori, "Boundary film formation from overbased calcium sulfonate additives during running-in process of steel-DLC contact," *Wear*, vol. 265, no. 3–4, pp. 461–467, 2008, doi: 10.1016/j.wear.2007.11.027.

[35]   S. Kosarieh, A. Morina, E. Lainé, J. Flemming, and A. Neville, "Tribological performance and tribochemical processes in a DLC / steel system when lubricated in a fully formulated oil and base oil," *Surf. Coat. Technol.*, vol. 217, pp. 1–12, 2013, doi: 10.1016/j.surfcoat.2012.11.065.

[36]   G. Vaitkunaite, Vaitkunaite, C. Espejo, C. Wang, B. Thiébaut, C. Charrin, A. Neville, A. Morina, "MoS2 tribofilm distribution from low viscosity lubricants and its effect on friction," *Tribol. Int.*, vol. 151, no. June, 2020, doi: 10.1016/j.triboint.2020.106531.

[37]   J. Graham, H. Spikes, and S. Korcek, "The friction reducing properties of molybdenum dialkyldithiocarbamate additives: part i — factors influencing friction reduction," *Tribol. Trans.*, vol. 44, no. 4, pp. 626–636, 2001, doi: 10.1080/10402000108982504.

[38]   J. D. Forero, G. V. Ochoa, and W. P. Alvarado, "Study of the piston secondary movement on the tribological performance of a single cylinder low-displacement diesel engine," *Lubricants*, vol. 8, no. 11, pp. 1–32, 2020, doi: 10.3390/lubricants8110097.

[39]   H. Murakami, N. Nakanishi, N. Ono, and T. Kawano, "New three-dimensional piston secondary motion analysis method coupling structure analysis and multi body dynamics analysis," *SAE Tech. Pap.*, vol. 5, no. 1, 2011.

[40]   M. M. Shuster, T. Stong, M. C. Deis, and D. C. Burke, "Piston ring cylinder liner scuffing phenomenon: Investigation, simulation and prevention," *SAE Tech. Pap.*, no. 724, 1999, doi: 10.4271/1999-01-1219.

[41]   A. R. Konicek, P. W. Jacobs, M. N. Webster, and A. M. Schilowitz, "Role of tribofilms in wear protection," *Tribol. Int.*, vol. 94, pp. 14–19, 2016, doi: 10.1016/j.triboint.2015.08.015.

[42]   R. Heuberger, A. Rossi, and N. D. Spencer, "XPS study of the influence of temperature on ZnDTP tribofilm composition," *Tribol. Lett.*, vol. 25, no. 3, pp. 185–196, 2007, doi: 10.1007/s11249-006-9166-9.

[43]   S. R. Bewsher, M. Leighton, M. Mohammadpour, H. Rahnejat, G. Offner, and O. Knaus, "Boundary friction characterisation of a used cylinder liner subject to fired engine conditions and surface deposition," *Tribol. Int.*, vol. 131, no. July 2018, pp. 424–437, 2019, doi: 10.1016/j.triboint.2018.11.005.